# Global DNA Methylation and Histone Posttranslational Modifications in Human and Nonhuman Primate Brain in Association with Prenatal Alcohol Exposure

Jessica S. Jarmasz, Hannah Stirton, Duaa Basalah, James R. Davie, Sterling K. Clarren, Susan J. Astley, and Marc R. Del Bigio

**Background:** Based upon experimental animal studies, the neurodevelopmental abnormalities associated with prenatal alcohol exposure (PNAE)/fetal alcohol spectrum disorder (FASD) have been attributed, at least in part, to epigenetic modifications. However, there are no direct analyses of human brain tissue.

**Methods:** Immunohistochemical detection of global epigenetic markers was performed on temporal lobe samples of autopsied fetuses and infants with documented PNAE. They were compared to age-, sex-, and postmortem delay-matched control cases (18 pairs; 20 to 70.5 weeks postconception). Temporal lobe tissue from a macaque monkey model of PNAE was also studied (5.7 to 6 months of age). We used antibodies targeting 4 DNA cytosine, 4 histone methylation, and 6 histone acetylation modifications and assigned scores based upon the semiquantitatively graded intensity and proportion of positively labeled nuclei in the ventricular and subventricular zones, ependyma, temporal cortex, temporal white matter, dentate gyrus (DG), and CA1 pyramidal layer.

**Results:** Temporal changes were identified for almost all marks according to the state of maturation in the human brain. In the DG (and 3 other brain regions), a statistically significant increase in H3K9ac was associated with PNAE. Statistically significant decreases were seen among 5mC, H3K4me3, H3K9ac, H3K27ac, H4K12ac, and H4K16ac in select regions. In the macaques, H3K36me3 decreased in the DG, and the ependyma showed decreases in 5fC and H3K36me3.

**Conclusions:** In human brain, global intranuclear epigenetic modifications are brain region and maturation state-specific. These exploratory results support the general hypothesis that PNAE is associated with a global decrease in DNA methylation, a global decrease in histone methylation, and a global increase in histone acetylation. Although the human and monkey subjects are not directly comparable in terms of brain maturation, considering the rapid temporal changes in global epigenetic modifications during brain development, interspecies comparisons may be extremely difficult.

**Key Words:** Acetylation, Methylation, Epigenetics, Human Brain, Prenatal Alcohol.

An estimated 10 to 15% of women in North America consume alcohol (ethanol) during pregnancy (Popova et al., 2017). Prenatal alcohol exposure (PNAE) is associated with spontaneous abortion, sudden unexplained death of an infant (SUDI), and fetal alcohol spectrum disorder (FASD). Individuals with FASD demonstrate neurodevelopmental malformations, cognitive deficits, and social and behavioral problems (Carson et al., 2010; Reynolds et al., 2011). The global prevalence of FASD is estimated to be 7.7 per 1,000 people (Lange et al., 2017), and it is considered one of the most common causes of neurodevelopmental abnormalities (Popova et al., 2012).

In individuals diagnosed with FASD, neuroimaging studies (MRI) have demonstrated a wide range of brain

*From the, Department of Pathology (JSJ), University of Manitoba, Winnipeg, Manitoba, Canada; Max Rady College of Medicine (HS), University of Manitoba, Winnipeg, Manitoba, Canada; Department of Pathology (DB), University of Manitoba, Winnipeg, Manitoba, Canada; Department of Biochemistry and Medical Genetics (JRD), University of Manitoba, Winnipeg, Manitoba, Canada; Department of Pediatrics (SKC), University of Washington School of Medicine, Seattle, Washington, USA; Department of Pediatrics (SKC), University of British Columbia Faculty of Medicine, Vancouver, British Columbia; Departments of Epidemiology/Pediatrics (SJA), University of Washington, Seattle, Washington; and Department of Pathology (MRDB), University of Manitoba, Winnipeg, Manitoba, Canada.*

*Received for publication January 8, 2019; revised February 26, 2019; accepted March 25, 2019.*

*Reprint requests: Marc R. Del Bigio, MD, PhD, Department of Pathology, University of Manitoba, Room 401 Brodie Centre – 727 McDermot Avenue, Winnipeg, MB, R3E 3P5, Canada; Tel.: 204-789-3378; Fax: 204-789-3931; E-mail: marc.delbigio@umanitoba.ca*

*Current address: Duaa Basalah, Royal Commission Medical Center, Yanbu, Saudi Arabia*



**DOI: 10.1111/acer.14052**

abnormalities including micrencephaly, abnormal gyral patterns, corpus callosum abnormalities, cortical thinning, and reductions in regional brain volume (e.g., basal ganglia, diencephalon, and cerebellum; Donald et al., 2015; Jacobson et al., 2017; Moore et al., 2014; Nardelli et al., 2011; Norman et al., 2009). In our recent descriptive study of 174 human autopsy cases (fetuses, infants, children, teens, and adults) with PNAE or FASD, we identified 31 cases with micrencephaly, 6 cases with simple hydrocephalus, 6 with corpus callosum defects, 5 with neural tube defects, 5 with prenatal ischemic lesions, and 4 cases with heterotopias (Jarmasz et al., 2017).

The pathogenesis of PNAE/FASD-associated brain anomalies is not well understood. Many molecular studies in animals suggest that epigenetic modifications are involved (Chater-Diehl et al., 2017; Lussier et al., 2017). Epigenetics includes a range of acquired and inheritable chemical modifications found within and surrounding (i.e., histones) the genome that influences gene expression without direct changes to the nucleotide sequence of DNA (Feinberg, 2018). Epigenetics plays a substantial role in DNA replication and transcription, genomic imprinting, cellular differentiation, and cell death. Epigenetic processes include chromatin remodeling, RNA interference (micro RNAs), and covalent reversible chemical modifications to DNA (DNA cytosine modifications) or to histones (posttranslational modifications—PTMs; Feinberg, 2018). Recent reviews have summarized the epigenetic effects, mainly DNA methylation and histone posttranslational modifications (PTMs), in the brains of rodents exposed to alcohol in the pre- and postnatal (human third trimester equivalent) periods (Chater-Diehl et al., 2017; Laufer et al., 2017; Lussier et al., 2017). For a summary of PNAE epigenetic studies that studied the brain specifically, see Appendix S1.

Within the central nervous system, differentiation of neural stem/precursor cells into neurons, astrocytes, and oligodendrocytes is epigenetically driven (Coskun et al., 2012; Hirabayashi and Gotoh, 2010; Liu et al., 2016). For example, neural genes are activated through histone acetylation, whereas pluripotent genes and nonneural genes are repressed through histone methylation and DNA methylation (Hirabayashi and Gotoh, 2010).

To the best of our knowledge, PNAE-associated epigenetic changes have not been directly assessed in human brain tissue. In this study, temporal lobe and hippocampus samples from 18 prenatal alcohol-exposed fetuses and infants who had undergone autopsy (Jarmasz et al., 2017) were compared to age-matched controls using immunohistochemical detection of 4 DNA cytosine modifications, 4 histone methylation modifications, and 6 histone acetylation modifications. In parallel, we studied the temporal lobes from macaque monkey infants that had been exposed in utero to alcohol (Clarren et al., 1987, 1990). We hypothesized that PNAE is associated with global epigenetic changes that persist postnatally in the nuclei of brain cells.

## MATERIALS AND METHODS

### *Human Autopsy Cases*

Ethics approval was obtained from the University of Manitoba Research Ethics Board (#HS1311 – H2011:213). Details of the full PNAE/FASD autopsy cohort ($N = 174$) were described previously (Jarmasz et al., 2017). Because our hypothesis concerns epigenetic changes associated with PNAE, and because epigenetic changes can occur during postnatal life (Kundakovic and Champagne, 2015), we restricted our study to fetuses and infants <1 year. Exclusion criteria were as follows: documented in utero alcohol consumption by the mother in the clinical history of the autopsy report (see Jarmasz et al., 2017; for more details), no availability of formalin-fixed paraffin-embedded (FFPE) brain sample(s), extensive autolysis of brain tissue, severe hypoxic damage, cases dated <1988 (inconsistent FFPE), known gene mutations or chromosomal abnormalities, major brain malformations, bacterial meningitis, and a postmortem delay (PMD) > 48 hours. In our recent study, a PMD of >48 to 72 hours in pig and mouse brain tissue had adverse effects on histone acetylation marks (Jarmasz et al., 2019). When these histone acetylation marks were tested in a human brain microarray containing brain samples with PMDs of 96 and 120 hours, stability was >96 hours (Jarmasz et al., 2019). Age- and sex-matched controls were selected from the same autopsy database. Sex matching is important because there are documented differences in brain size, neurological disease prevalence, epigenetics, and stress response (Dekaban, 1978; Kigar and Auger, 2013; Menger et al., 2010; Shen et al., 2015). Inclusion criteria for age- and sex-matched controls were as follows: The case year had to be accrued within 10 years of the PNAE case, suffered little to no brain trauma, had no brain abnormalities, had no clinical history of prenatal alcohol or drug exposure, and had a PMD of ≤48 hours. A recent fetal case not described in the previous publication (Jarmasz et al., 2017) was included because the documented PNAE exposure was high despite not meeting the ≤48-hours PMD inclusion criteria. The PNAE cohort consisted of 9 fetuses or premature births with gestational age < 42 weeks and 9 infants age 43 to 70.5 weeks PC, along with controls. PNAE cohort epidemiologic and pathologic details are described in Table 1. PNAE and control pairings are described in Table 2. FFPE medial temporal lobe blocks stored at the pathology department (Health Sciences Centre, MB) were cut by microtome (5 to 6 $\mu$m thick) and mounted onto charged slides for immunohistochemistry.

### *Nonhuman Primate PNAE Brains*

The *Macaca nemestrina* PNAE study was conducted in the 1980s (Bonthius et al., 1996; Clarren et al., 1987, 1988, 1990; Sheller et al., 1988), in compliance with University of Washington Administrative Policy for the humane treatment of animals used in research. Briefly, 48 pregnant adult female pig-tailed macaques received once-weekly nasogastric doses of ethanol ranging from 0.3 to 4.1 g/kg bodyweight; the highest dose is roughly equivalent to 16 standard distilled liquor drinks in a human (i.e., a binge exposure). High doses (2.5, 3.3, and 4.1 g/kg weekly) of alcohol were started at 33 to 46 days of gestation, rather than the time of fertilization, to reduce the risk of spontaneous abortion (Clarren et al., 1987). Controls received isocaloric sucrose. Thirty-three viable infants were born and subsequently assessed for overall health and features of the fetal alcohol syndrome phenotype (Clarren et al., 1988). The monkeys were killed at 5.7 to 7.2 months of age (Clarren et al., 1990), which is the human brain development equivalent of 2.7 to 3.5 years of age (http://translatingtime.org/translate). The cerebral hemispheres were bisected along the midsagittal plane and further dissected to produce multiple brain regions of interest for various studies. The right hemisphere was placed in 10% neutral buffered formalin for neuropathological study. After fixation (duration not documented),

**Table 1.** Clinical Details of Fetuses and Infants with Prenatal Alcohol Exposure

| Case no. | Sex | Age | Cause of death | Brain weight (percentile)[a] | PNAE | Physical anomalies | Cardiac defects | Brain abnormalities |
|---|---|---|---|---|---|---|---|---|
| 1 | F | 20 weeks' gestation | Stillborn/intrauterine death | ≥10th to <50th | Alcohol abuse | – | – | None |
| 2 | F | 21.5 weeks' gestation | Stillborn/intrauterine death | <5th | Rubbing alcohol 2nd trimester | None | None | Micrencephaly |
| 3 | M | 27 weeks' gestation | Stillborn/intrauterine death | ≥10th to <50th | Alcohol abuse | Facial anomalies, low-set ears, bilateral neck webbing | None | None |
| 4 | F | 29 weeks' gestation | Stillborn/intrauterine death | Not indicated | Alcohol abuse | Low-set ears | None | None |
| 5 | M | 34 weeks' gestation | Stillborn/intrauterine death | ≥5th to <10th | Drank until pregnancy was determined | Low-set ears, palmar creases unusual | None | Micrencephaly |
| 6 | F | 34 weeks' gestation | Intrapartum death with prematurity | <5th | Drank heavily throughout pregnancy | Facial anomalies, bilateral club foot and partial webbing of toes | Absent superior vena cava, large ASD | Micrencephaly, ventricle wall fusion (partial), periventricular heterotopia (rare), retarded laminar development cerebral cortex and hippocampus, hypoplasia pons |
| 7 | M | 36 weeks' gestation | Stillborn/intrauterine death | ≥10th to <50th | Occasional alcohol during the first trimester | None | Right coronary ostium | None |
| 8 | F | 40 weeks' gestation | Stillborn/intrauterine death with placental abnormalities | <5th | Drank heavily during the third trimester | None | None | Micrencephaly |
| 9 | M | 41 weeks' gestation | Stillborn/intrauterine death | <5th | History of alcohol abuse | None | None | Micrencephaly |
| 10 | M | 21 days (43 weeks PC) | Bacterial + viral infection | <5th | Drank throughout pregnancy | None | None | Micrencephaly |
| 11 | F | 23 days (43.5 weeks PC) | SUDI with unsafe sleeping environment | ≥5th to <10th | Drank throughout pregnancy | None | None | Micrencephaly |
| 12 | M | 6 weeks (46 weeks PC) | SUDI with congenital anomalies | ≥10th to <50th | Drank during pregnancy (known alcoholic) | Thin upper lip | ASD with PDA | Recent mild hypoxic neuron change. |
| 13 | F | 8 weeks (48 weeks PC) | SUDI with congenital anomalies | Not Indicated | Drank heavily during pregnancy | None | Small VSD | None |
| 14 | M | 2 months (48.5 weeks PC) | SUDI with unsafe sleeping environment | ≥10th to <50th | Drank during pregnancy | Low-set ears | Subaortic VSD | None |
| 15 | M | 3 months (53 weeks PC) | SUDI | ≥10th to <50th | Binged during pregnancy | None | None | None |
| 16 | F | 4 months (57.5 weeks PC) | SUDI | ≥10th to <50th | Drank during the first and second trimester | None | None | Periventricular leukomalacia, subacute (small foci in parietal white matter) |
| 17 | F | 6 months (66 weeks PC) | SUDI | ≥50th to <90th | Fetal alcohol syndrome | None | None | Polygyria |
| 18 | M | 7 months (70.5 weeks PC) | SUDI | >95th | Mother alcoholic | Facial anomalies | None | None |

PC, postconception; SUDI, sudden unexpected death of an infant.

[a]According to Maroun et al., 2005 *Pediatric and Developmental Pathology : The Official Journal of the Society for Pediatric Pathology and the Paediatric Pathology Society*. 8(2);204–17 and Phillips et al., 2009 *Pathology*. 41(6);515–26.

**Table 2.** Alcohol-Exposed Human Fetuses and Infants with Paired Control Cases

| | | Prenatal alcohol exposed | | | Age-, Sex-, and PMD-matched controls | | |
|---|---|---|---|---|---|---|---|
| Case no. | Sex | PMD (hours) | Age (PC weeks) | Cause of death | PMD (hours) | Age (PC weeks) | Cause of death |
| 1 | F | 24 | 20 weeks | Stillborn/intrauterine death | <24 | 21 weeks | Stillborn/intrauterine death with placental abnormalities |
| 2 | F | 24.5 | 21.5 weeks | Stillborn/intrauterine death | 21.5 | 22 weeks[a] | Intrapartum death: prematurity |
| 3 | M | 7 to 8.5 | 27 weeks | Stillborn/intrauterine death | 22 | 25 weeks | Stillborn/intrauterine death with placental abnormalities |
| 4 | F | 49 | 29 weeks | Stillborn/intrauterine death | ~24 | 31 weeks | Stillborn/intrauterine death with placental abnormalities |
| 5 | M | ~24 | 34 weeks | Stillborn/intrauterine death with malformation(s) | 56.5 | 33 weeks | Prematurity with pulmonary hypoplasia |
| 6 | F | 107 | 34 weeks[a] | Intrapartum death: prematurity and malformation(s) | 48 | 34 weeks[a] | Intrapartum death: prematurity and malformation(s) |
| 7 | M | 48 | 36 weeks | Stillborn/intrauterine death | ~1 to 5 | 37.5 weeks | Stillborn/intrauterine death |
| 8 | F | 33 | 40 weeks | Stillborn/intrauterine death with placental abnormalities | 32 | 38 weeks | Stillborn/intrauterine death |
| 9 | M | 39 | 41 weeks | Stillborn/intrauterine death | ~39 to 49 | 40 weeks | Stillborn/intrauterine death |
| 10 | M | 28 | 43 weeks | Bacterial/viral infection | 24 to 30 | 43 weeks | SUDI due to unsafe sleeping environment |
| 11 | F | 20 | 43.5 weeks | SUDI due to unsafe sleeping environment | 49 | 44 weeks | Asphyxiation due to accidental smothering |
| 12 | M | 21 | 46 weeks | Malformations/congenital anomalies | 26 | 46 weeks | SUDI due to unsafe sleeping environment |
| 13 | F | 12 | 48 weeks | Malformations/congenital anomalies | 24 | 48 weeks | SUDI |
| 14 | M | 25 to 35 | 48.5 weeks | SUDI due to unsafe sleeping environment | 47 to 53 | 48.5 weeks | SUDI due to unsafe sleeping environment |
| 15 | M | 26 | 53 weeks | SUDI | 36 | 53 weeks | SUDI |
| 16 | F | 3.5 to 7.5 | 57.5 weeks | SUDI | ~24 | 57.5 weeks | SUDI |
| 17 | F | 8 | 66 weeks | SUDI | 24 to 36 | 64 weeks | SUDI due to unsafe sleeping environment |
| 18 | M | 19.5 | 70.5 weeks | SUDI | 32 to 34 | 70.5 weeks | Accidental positional asphyxiation |

F, Female; M, Male, PC, Postconception; PMD, Postmortem delay; SUDI, Sudden unexplained death of an infant.
[a]Liveborn; died within minutes to hours of birth.

the hemisphere was divided into 5 mm coronal slices and embedded in paraffin (Clarren et al., 1990). Blocks of FFPE tissue, which had been archived at the University of Washington, were transferred to the senior author's (MRD) laboratory. The available samples consisted of 6 to 8 coronal slices of 1 cerebral hemisphere extending from the occipital lobe tip to the frontal lobe at the level of the posterior striatum. In all cases, at least 1 slice included temporal lobe, hippocampus, thalamus, and posterior putamen. Because the paraffin was brittle, tissue blocks of interest were heated at 60°C for 30 minutes and reembedded in new paraffin. We used only the 3 highest PNAE levels (2.5, 3.3, and 4.1 g/kg; $N = 6$) along with controls (sucrose exposure only; $N = 5$; Appendix S2).

### *Antibodies to Epigenetic Modifications*

We selected antibodies that detect epigenetic modifications known to occur in the brain, and/or have been reported to be affected by alcohol exposure in the prenatal, postnatal immature, or adult periods in either human brain cell lines or rodent brains (Chater-Diehl et al., 2017; Laufer et al., 2017; Lussier et al., 2017). These include 5-methylcytosine (5mC), 5-hydroxymethylcytosine (5hmC), 5-formylcytosine (5fC), 5-carboxycytosine (5caC), histone trimethylated at lysine 4 (H3K4me3), H3K9me2/K9me3, H3K27me3, H3K36me3, histone acetylated at lysine 9 (H3K9ac), H3K14ac, H3K27ac, H4K5ac, H4K12ac, and H4K16ac. We also included antibodies targeting total histone H3 and H4, as well as pan-acetyl H3 and H4. Rationale for inclusion of DNA/histone modifications in this study and technical details of the epigenetic antibodies are presented in Appendix S3 and Table 3. Antibody specificity and epitope tolerance to postmortem degradation is described in detail in a recent publication (Jarmasz et al., 2019).

### *Immunohistochemistry*

Human and macaque brain tissue sections (5 to 6 $\mu$m thickness) were subjected to immunohistochemistry, which is described in detail in a recent publication (Jarmasz et al., 2019). Optimal primary antibody concentration was determined by running a series of dilutions greater and less than the manufacturers' suggestions (Appendix S4). Briefly, paraffin was melted at ~60°C, and tissue samples were rehydrated through multiple xylenes and graded ethanol solutions (100, 90, and 75%). Slides were subjected to antigen retrieval, as well as endogenous peroxidase blocked before incubation with 10% serum. The primary antibody was applied, followed by application of the secondary antibody, followed by application of peroxidase-conjugated streptavidin (with multiple 4-minute washes in-between each application). DAB (3,3′ diaminobenzidine) chromogen was used to develop the slides. The slides were counterstained with Harris hematoxylin solution, dehydrated through graded ethanol and multiple xylene solutions, coverslipped with Permount, and left to air-dry overnight.

### *Imaging of Immunohistochemical Results*

Human and macaque slides were imaged using a standard upright microscope with digital camera (Olympus BX51TRF microscope, Olympus Scientific Solutions, Waltham, MA; Qimaging 32-0110A-568 MicroPublisher 5.0, Model LH100HG, Teledyne

**Table 3.** Details and Sources for the Antibodies to Epigenetic Marks

| Antibody | Immunogen/target | Isotype | Species | Type | Company details | Lot no. |
|---|---|---|---|---|---|---|
| 5mC | Recognizes 5-methylcytidine in vertebrate DNA | IgG | Mouse | Monoclonal (clone 33D3) | Active Motif, #39649 | 24516019 |
| 5hmC | Raised against 5-hydroxymethylcytosine conjugated to KLH | Serum | Rabbit | Polyclonal | Active Motif, #39769 | 06116002 |
| 5fC | Raised against 5-formylcytidine conjugated to KLH | Serum | Rabbit | Polyclonal | Active Motif, #61223 | 34711001 |
| 5caC | Raised against 5-carboxycytosine conjugated to KLH | Serum | Rabbit | Polyclonal | Active Motif, #61225 | 32115002 |
| H3K4me3 | Raised against a peptide including trimethyl-lysine 4 of histone H3. | Serum | Rabbit | Polyclonal | Active Motif, #39159 | 12613005 |
| H3K9ac | Synthetic peptide corresponding to Human Histone H3 aa 1-100 (N-terminal) (acetyl K9) conjugated to KLH | IgG | Rabbit | Polyclonal | Abcam, #ab10812 | GR287797-1 |
| H3K9me2, K9me3 | Synthetic peptide within human histone H3 aa1-100 (tri methyl K9); exact sequence is proprietary | IgG1 | Mouse | Monoclonal (clone 6F12-H4) | Abcam, #ab71604 | GR117765-1 |
| H3K14ac | Synthetic peptide within human histone H3 (acetyl K14); exact sequence is proprietary. | IgG | Rabbit | Monoclonal (clone EP964Y) | Abcam #ab52946 | GR302893-8 |
| H3K27ac | Synthetic peptide corresponding to human histone H3 aa 1-100 (acetyl K27) conjugated to KLH | IgG | Rabbit | Polyclonal | Abcam, #ab4729 | GR288020-1 |
| H3K27me3 | Synthetic peptide within human histone H3 aa 1-100 (tri methyl K27) conjugated to KLH; exact sequence is proprietary | IgG | Mouse | Monoclonal (clone 6002) | Abcam, #ab6002 | GR275911-7 |
| H3K36me3 | Synthetic peptide within human histone H3 aa 1-100 (tri methyl K36) conjugated to KLH; exact sequence is proprietary | IgG | Rabbit | Polyclonal | Abcam, #ab9050 | GR3177961-1 |
| H4K5ac | Synthetic peptide within human histone H4 aa 1-100 (N-terminal) (acetyl K5); exact sequence is proprietary | IgG | Rabbit | Monoclonal (clone EP1000Y) | Abcam, #ab51997 | GR295999-7 |
| H4K12ac | Synthetic peptide corresponding to human histone H4 aa 10-15 (acetyl K12) | IgG | Rabbit | Polyclonal | Abcam, #ab61238 | GR325039-3 |
| H4K16ac | Synthetic peptide corresponding to human histone H4 (acetyl K16); exact sequence is proprietary | IgG | Rabbit | Monoclonal (EPR1004) | Abcam, #ab109463 | GR187780-8 |
| H3panAc | Peptide including acetyl-lysines contained in the N-terminal tail of human histone H3 | IgG | Rabbit | Polyclonal | Active Motif, #61637 | 28915002 |
| Total H3 | Peptide containing the N-terminus of histone H3. | IgG2b | Mouse | Monoclonal (clone MABIO3O1) | Active Motif, #39763 | 34614001 5217020 |
| Total H4 | Synthetic peptide containing human histone H4. | IgG2b | Mouse | Monoclonal (clone MABI0400 | Active Motif, #61521 | 7715006 |

KLH, keyhole limpet hemocyanin.

Qimaging, Surrey BC, Canada). Images were captured at 40×, 200×, or 400× total magnification using QCapture software (v2.8.1, 2001 to 2005, Qimaging Corp., Teledyne Qimaging, Surrey BC, Canada). The dentate gyrus (DG), CA1 neurons of the hippocampal formation (CA1), ependymal cells along the floor of the temporal horn of the lateral ventricle, temporal neocortex (CX) in the parahippocampal gyrus, and temporal white matter (WM) were evaluated. In human fetuses 34 weeks and younger, the germinal region along the roof of the lateral ventricle, including the ventricular zone (VZ) and subventricular zones (SVZ), was also evaluated. Two previously validated (Jarmasz et al., 2019) semiquantitative scales were used to score the estimated proportion of immunoreactive nuclei (graded 0 to 4; corresponding to approximately 0, 25, 50, 75, and 100% positive) and the graded intensity of immunoreactivity in comparison with a standard image set (graded 0 to 3.5 in 0.5 steps; see Additional file 13, in Jarmasz et al., 2019). Morphologic features of nuclei were used as a surrogate for probable brain cell type. Cells with large round nuclei and prominent nucleoli were considered as probable neurons; cells with medium-sized round or irregular nuclei were considered probable astrocytes (in WM) or possible small neurons in cortex; cells with small round nuclei were considered probable oligodendrocytes; cells with small elongated and irregular nuclei were considered probable microglia; cells with small elongated smooth-contoured nuclei near a vascular lumen were considered endothelial; and cells wrapping vascular endothelia were considered to be smooth muscle. First, control cases were examined in order to establish a general developmental pattern of expression for the epigenetic marks. Second, matched pairs of control and PNAE cases were compared in all brain regions. Not all epigenetic marks were evaluated in every single case. For example, focal tissue damage or imperfections in the immunostaining would preclude proper evaluation. The immunoreactivity scores (proportion and intensity grades) for every brain region were recorded in a Microsoft Excel spreadsheet.

### *Statistical Analyses*

The multiplied proportion and intensity scores were graphed as a function of age for each anatomical region and presented as bar graphs using Microsoft Excel ($Y$-axis = total multiplied rank, $X$-axis = postconception age in weeks). Third-order polynomial trendlines ($y = (m_3{*}x^3 + m_2{*}x^2 + m_1{*}x) + b$) were superimposed to the graphed values to depict the general pattern of developmental expression for each epigenetic mark. PNAE data curves were added

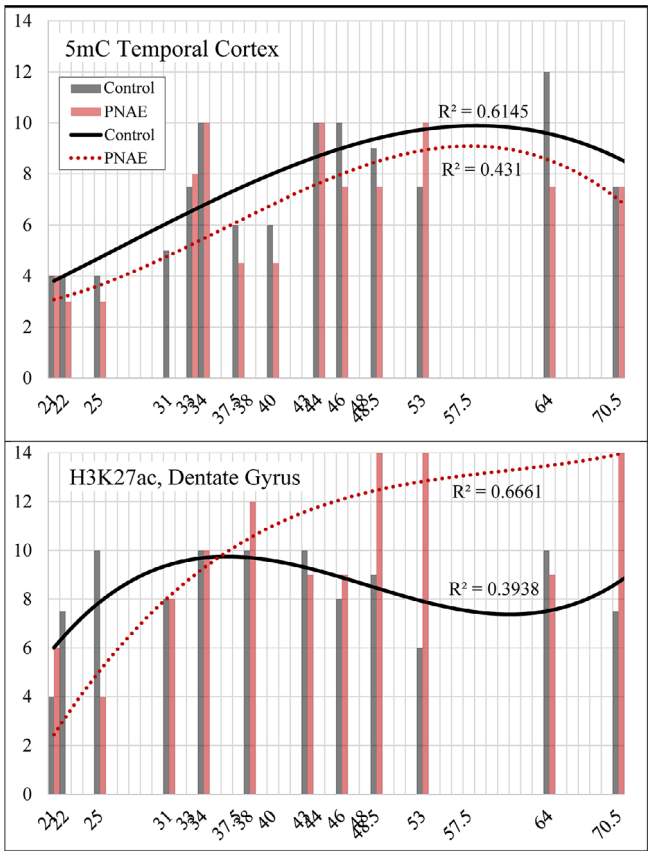


**Fig. 1.** Examples of human control and PNAE immunostaining scores with third-order polynomial curve fit with $R^2$ values. The gray bars and black solid curve represent controls, and the red bars and dotted curve represent PNAE cases. The *Y*-axis shows the semiquantitative scores, which is the product of intensity and distribution scores multiplied (maximum score of 14). The *X*-axis is the postconception age in weeks.

to highlight possible differences (Fig. 1). Goodness of fit ($R^2$) is shown on the graphs; the average $R^2$ value was 0.5352 ± 0.0246 (mean $R^2$ ± SEM) for controls and 0.5575 ± 0.0254 for PNAE. However, because the data represent 2 biologically different populations (i.e., stillborn fetuses with uncertain postmortem in utero conditions vs. liveborn infants) a formal polynomial regression fit to compare the curves is likely not valid. Data were subjected to multiple paired *t*-test (2-tailed) comparisons (JMP 14.1 statistical software; SAS Institute, Cary, NC) within 6 age clusters: 21 to 25 weeks PC ($n$ = 3 pairs) and 31 to 34 weeks PC ($n$ = 3 pairs) for the VZ and SVZ; 21 to 25 weeks PC ($n$ = 3 pairs; early fetus), 31 to 40 weeks PC ($n$ = 6 pairs; late fetus), 43 to 48.5 weeks PC ($n$ = 5 pairs; young infant), and 53 to 70.5 weeks PC ($n$ = 4 pairs; infants) for all remaining brain regions. As recommended for exploratory research, all p values are reported without correction for multiple tests (13 antibodies, 5 brain loci), acknowledging that $p$ values marginally <0.05 should be interpreted with caution (Bender and Lange, 2001; Cipriani et al., 2015).

For the macaque brains, images were scored as described above. The Wilcoxon Rank Sums test with chi-square approximation (Kruskal–Wallis) was used to compare control and PNAE groups for each location and each antibody (JMP 14.1 statistical software; SAS Institute). The $p$ values were manually adjusted using the Benjamini–Hochberg formula (Benjamini and Hochberg, 1995): $((i/m)*Q)$ and a false discovery rate (FDR) of 0.1. Those $p$ values that did not remain significant after the Benjamini–Hochberg correction but were still below 0.05 are reported as trends.

## RESULTS

### *General Observations Concerning Immunohistochemical Labeling of Histone Modifications*

Most of the antibodies yielded strong and consistent immunolabeling in both human and monkey tissues. We had originally intended to study antibodies targeting total histone H3, total histone H4, pan-acetyl histone H3, pan-acetyl histone H4, H3K9me2, and H3K27me2. For total histone H3 and H4 antibodies, we expected the antibodies to label virtually every nucleus at all stages of maturation. Surprisingly, this was not the case (Appendix S5: Fig. 1). Similarly, we expected that histone H3 and H4 pan-acetyl antibodies would label more cells than any antibody targeting a single acetylated lysine. However, the proportion of cells labeled by anti-pan-acetyl histone H3 and H4 was much less than that labeled by single acetylation marks (Appendix S5: Fig. 1). Consequently, results of these are not reported. The H3K27me2 antibody binding was not blocked by the appropriate peptides. We were unable to get satisfactory cell labeling using the H3K9me2 antibody.

### *Developmental Expression of Epigenetic Modifications in Control Human Brain*

Graphic representations of the human control and PNAE results are shown in Figs 2–6. Polynomial curves were fitted to the data for all location/epitope combinations; they provide a convenient way for visualizing and comparing the data sets.

### *Ventricular and Subventricular Zones*

Developmental expression of epigenetic marks in the VZ varied considerably; 7/13 epigenetic marks (5mC, 5hmC, H3K36me3, H3K9ac, H3K14ac, and H4K5ac) exhibited a "U-" shaped expression curve prior to disappearance of the VZ at 31 to 34 weeks (Figs 2–5, 7; Appendix S5: Fig. 2). Note, however, that the sample sizes are small so we cannot be certain that the transient decline is real. In the SVZ, most marks started at low levels and increased with gestational age (5caC, H3K4me3, H3K36me3, H3K9ac, H4K5ac, and H4K12ac) (Figs 2–5; Appendix S5: Fig. 2). Within the SVZ, an anatomical gradient was evident for 5mC, H3K4me3, H3K36me3, H3K9ac, H3K14ac, H3K27ac, H4K5ac, H4K12ac, and H4K16ac; in the youngest fetuses, only the SVZ adjacent to the VZ was positive, followed by spreading to involve the entire SVZ prior to involution. Within the SVZ, there are different progenitor cell types (Rushing and Ihrie, 2016); however, they could not be easily distinguished due to similarity in size and morphology.

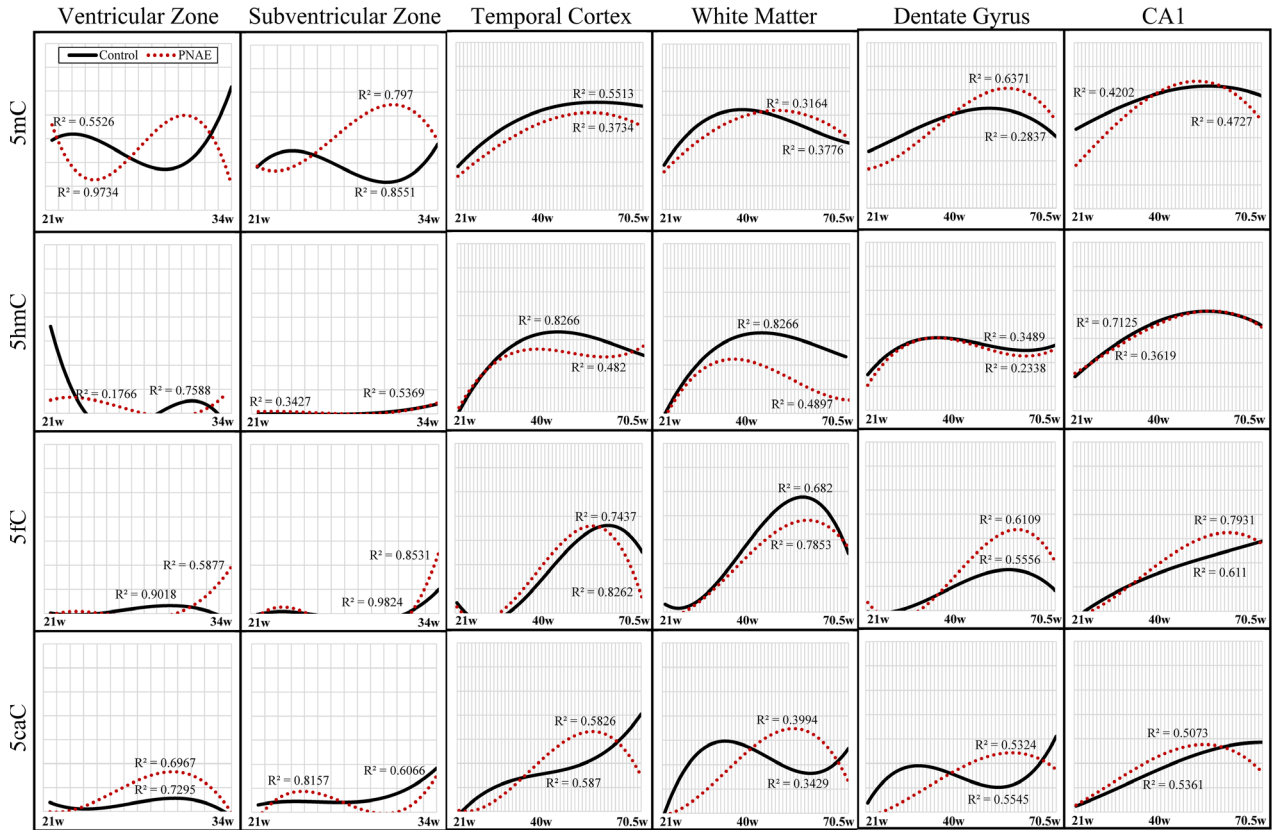


**Fig. 2.** Graphic representation of semiquantitative score values (maximum 14; *Y*-axis) for DNA cytosine modifications in the human brain regions assessed. The black curve represents the control cases, and the red dotted curve represents PNAE. Curve fit values ($R^2$) are also shown. The *X*-axis represents the postconception age in weeks. The ventricular (VZ) and subventricular zones (SVZ) are only present in fetal cases up to 34 weeks' gestation. In the VZ and SVZ, 5mC levels were highest, while 5hmC, 5fC, and 5caC levels were low. In the other brain regions, 5mC, 5hmC, and 5caC (white matter only) show a gradual increase, peaking at birth, followed by a plateau or decrease. Although the control and PNAE curves diverged in some circumstances, only 5mC in the CA1 sector of the early fetal PNAE group showed a statistically significant decrease ($p = 0.0198$).

### *Brain Surface and Temporal Neocortex*

Most epigenetic mark antibodies strongly labeled a narrow band of cells along the external surface from the earliest age studied (21 weeks; Fig. 8). This likely represents the marginal zone progenitor layer (Costa et al., 2007). The exceptions were anti-5mC and anti-5hmC, which showed only faint immunoreactivity in this location. In increasing maturity in fetal brains, epigenetic marks expressed in the cortical mantle tended to progress to increasing depths from the surface. Brain cell types were distinguishable through morphology with increasing age. Within the 5th and 6th cortical layers, all but 4 epigenetic marks (5fC, 5caC, H3K14ac, and H4K16ac) demonstrated ~75 to 100% positive staining among large (presumably neuronal) and intermediate-sized nuclei. In WM, small round (presumably oligodendroglial) nuclei demonstrated low positive proportions (≤50%) in the fetuses. In the infant cases, all marks except H3K4me3, H3K27ac, and H4K12ac increased to include ~50 to 100% of the presumptive oligodendrocytes. Epigenetic mark immunoreactivity varied considerably in presumed microglial nuclei. Active transcription marks (H3K4me3, H3K36me3, H3K27ac, H4K5ac, and H4K12ac) were most strongly expressed. Vascular endothelial cells and arterial smooth muscle cells had a seemingly random mix of positive and negative cells for most marks; the exceptions were almost uniform negativity for 5mC, 5hmC, 5fC, 5caC, and H4K16ac (Appendix S5: Fig. 3). Almost every antibody labeled choroid plexus epithelial cell nuclei (Appendix S5: Fig. 3).

### *White Matter*

In presumed oligodendrocytes (small round nuclei), most epigenetic marks were more widespread and more strongly immunoreactive in infants than in fetuses; exceptions were H3K27me3, H3K27ac, and H4K12ac, which decreased in infancy. Among larger irregular (presumed astroglial) nuclei, H4K5ac and H4K12ac were expressed in ~100% of cells at all ages examined. All other epigenetic marks were present in a minority (~0 to 50%) of cells during the fetal stages and increased to a ~50 to 100% in infancy. Among the few very large nuclei of presumed WM neurons, stable immunoreactivity was seen for all epigenetic marks except for 5fC, 5caC, H3K14ac, and H4K16ac, which were negligible in early fetuses (21 to 25 weeks PC) but attained positivity in infancy (53 to 70.5 weeks PC).

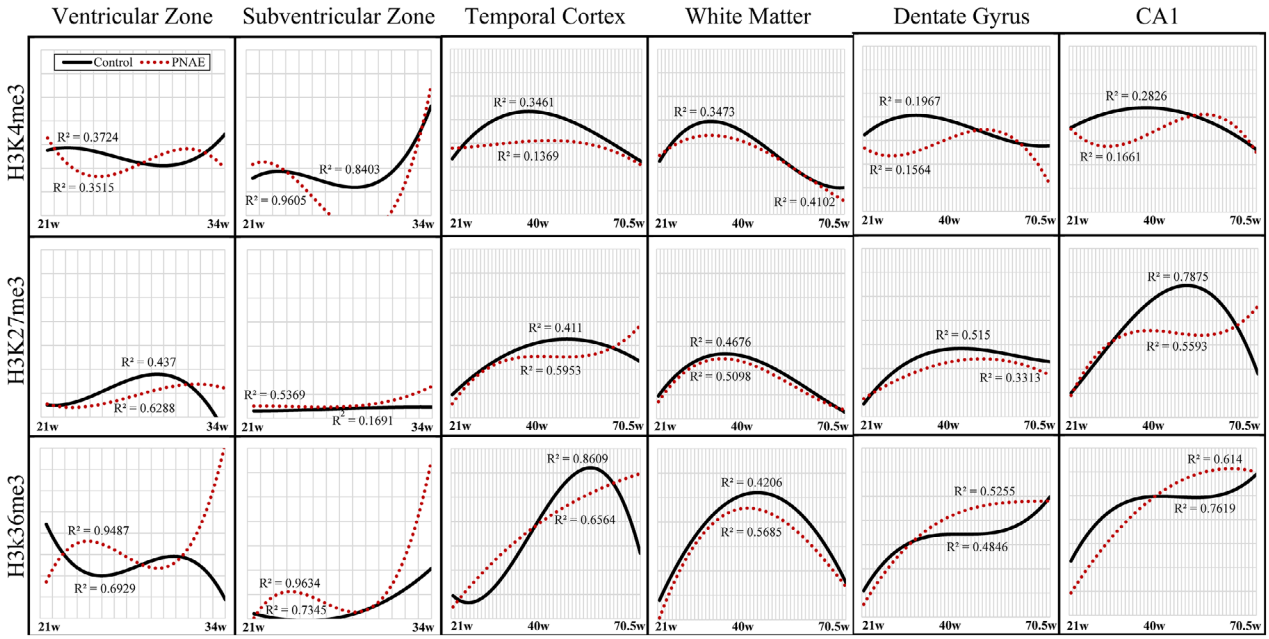


**Fig. 3.** Graphic representation of semiquantitative score values (maximum 14; *Y*-axis) for histone H3 methylation marks in the human brain regions assessed. The black curve represents the control cases, and the red dotted curve represents PNAE. Curve fit values ($R^2$) are also shown. In the control VZ, H3K4me3 was relatively stable while the other 2 declined with maturation. In the control SVZ, H3K27me3 was relatively stable while the other 2 increased with maturation. In all other brain regions, most of the marks showed a slight peak near birth. The exception was H3K36me3, which showed a steady increase in the DG and CA1 neurons. None of the histone methylation mark differences were statistically significant between PNAE and controls.

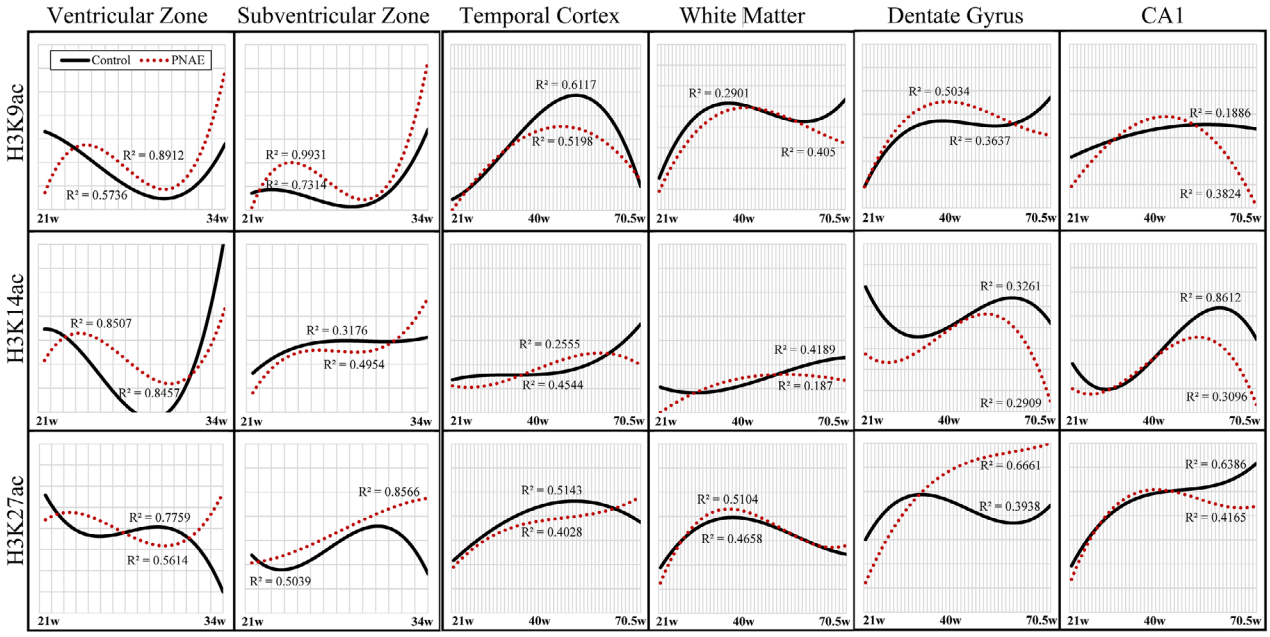


**Fig. 4.** Graphic representation of semiquantitative score values (maximum 14; *Y*-axis) for histone H3 acetylation marks in the human brain regions assessed. The black curve represents the control cases, and the red dotted curve represents PNAE. Curve fit values ($R^2$) are also shown. In the VZ and SVZ, H3K9ac and H3K14ac tended to increase with maturation while H3K27ac tended to decline. In the other brain regions, all of the marks tended to increase during the fetal period. Some differences were observed in association with PNAE. In the cortex, H3K9ac ($p = 0.0202$) and H3K27ac ($p = 0.0229$) were lower in young infants with PNAE. In the white matter, H3K9ac was lower ($p = 0.0377$) in the early fetal PNAE group compared with controls. In the dentate gyrus, H3K9ac was higher ($p = 0.0352$) in young PNAE infants. In the CA1, H3K27ac was lower ($p = 0.0414$) in PNAE infants.

### *Dentate Gyrus Neurons and Pyramidal Neurons of Hippocampal CA1 Region*

In human fetuses, granular neurons of the DG were ~50 to 75% positive for all epigenetic marks except for H3K27ac and H4K5ac, which were ~100% positive; the latter 2 are marks of active transcription. Almost all epigenetics marks increased in infancy except for 5hmC, 5fC, H3K4me3, and H4K5ac, which remained consistent. The proportion of CA1

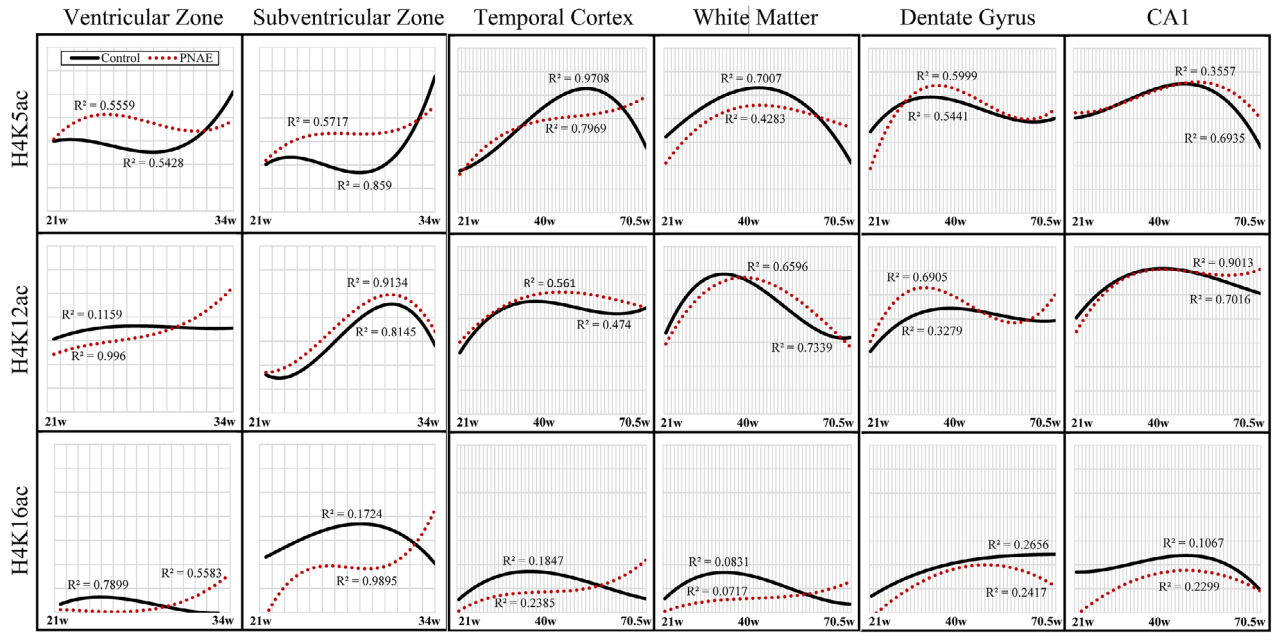


**Fig. 5.** Graphic representation of semiquantitative score values (maximum 14; *Y*-axis) for histone H4 acetylation marks in the human brain regions assessed. The black curve represents the control cases, and the red dotted curve represents PNAE. Curve fit values ($R^2$) are also shown. In the VZ and SVZ, H4K5ac tended to increase with maturation. In the other brain regions, most marks tended to increase during the fetal period and decrease during infancy. H4K16ac was significantly lower in the dentate gyrus ($p = 0.0339$) of young infants with PNAE.

pyramidal neurons immunoreactive for 5fC, 5caC, H3K14ac, and H4K16ac was low (~25 to 50%), while all other epigenetic marks were expressed in the majority of cells (~75 to 100%). Immunoreactivity for most epigenetic marks remained consistent from the fetal period to infancy. Exceptions were 5mC, 5fC, H3K4me3, H3K9ac, H3K14ac, and H4K16ac, which all increased (H4K16ac went from ~25% to ~100%).

### *Temporal Lobe Ependymal Cells*

For most epigenetic marks, nuclei of the temporal horn ependymal cells started at ~25 to 50% positive in fetuses and increased to ~75% positive in infants.

### *Differential Expression of Epigenetic Marks Between Brain Cell Types (see Appendix S6)*

In control and PNAE cases, all epigenetic marks except for 5fC, 5caC, H3K9ac, H3K14ac, and H4K16ac were identified in essentially all brain cell types. During the fetal period, almost all epigenetic marks were preferentially expressed in more mature cells that could be identified as neurons. 5hmC and H4K16ac appeared to be relatively specific to large hippocampal and cortical neurons. For 5mC, 5hmC, H3K27me3, H3K36me3, H3K9ac, and H4K16ac, the dentate neurons demonstrated a maturation gradient, where more mature nuclei distant from the germinal layer (i.e., distant from CA4 sector of the hippocampus) were positive, while less mature nuclei near the germinal layer were negative.

### *Comparison of Epigenetic Marks in Control and PNAE Brains*

Statistical comparisons between human control and PNAE pairings are summarized in Table 4. In the young fetuses, the VZ of PNAE cases had less H4K16ac immunoreactivity than controls ($p = 0.0039$). The temporal cortex (a mix of neurons and glial cells) of young infant PNAE cases had less H3K9ac ($p = 0.0202$) and H3K27ac ($p = 0.0229$) immunoreactivity than controls (Fig. 9). For both marks, the difference was reflected in intensity for all cell types, and specifically a loss of immunoreactivity in small round nuclei (presumably oligodendrocytes) for H3K27ac (Fig. 9). H3K9ac showed less immunoreactivity in PNAE WM ($p = 0.0377$; Fig. 10) and among the ependyma cells of the young fetuses ($p = 0.0198$; Fig. 11). Ependymal cells also exhibited decreases in intensity for H3K4me3 ($p = 0.0234$) and a decrease in the number of positive nuclei for H3K27ac ($p = 0.0142$) in the early fetal age group (Fig. 11). In the DG neurons of young infants, an increased intensity was observed for H3K9ac ($p = 0.0352$) (Fig. 10), and a decreased intensity was seen for H4K16ac. In the CA1 neurons of PNAE cases, a smaller proportion were 5mC positive ($p = 0.0198$) and reduced immunoreactivity was seen for H3K27ac ($p = 0.0414$). Overall, H3K9ac exhibited a notable difference in 4 of the 7 brain regions studied and appeared to be the only epigenetic mark affected by PNAE in both the human fetal and infant groups (Figs 9–11).

In the macaque brains, there were few statistically significant differences between the control and PNAE samples (Table 5). In the DG neurons of the PNAE group,

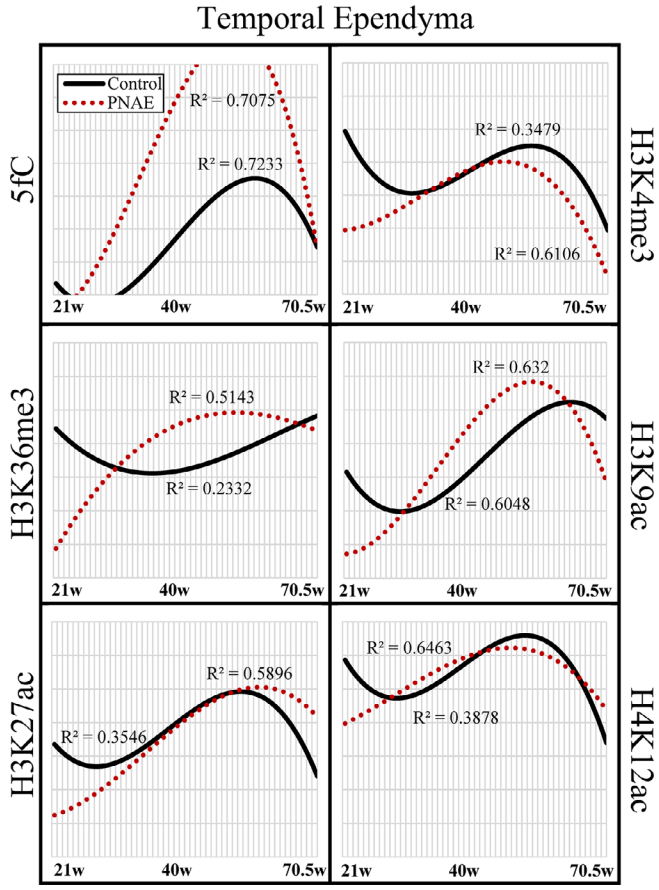


**Fig. 6.** Graphic representation of semiquantitative score values (maximum 14; *Y*-axis) in the human temporal ependyma. The black curve represents the control cases, and the red dotted curve represents PNAE. Curve fit values ($R^2$) are also shown. In the early fetal age group, H3K4me3 ($p = 0.0234$), H3K9ac ($p = 0.0198$), and H3K27ac ($p = 0.0142$) were all significantly lower in PNAE compared with controls.

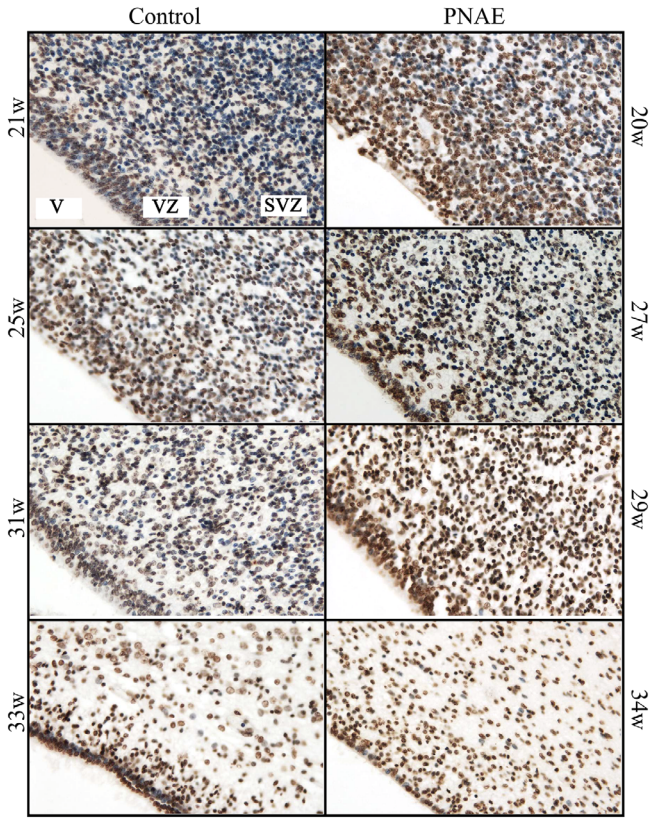


**Fig. 7.** Photomicrographs showing 5-methylcytosine (5mC) immunoreactivity in human ventricular (VZ) and subventricular zones (SVZ). In controls, most cells of the VZ are strongly positive until it is replaced by the ependymal layer at 31 to 34 weeks. Immunoreactivity in the SVZ increased slightly with fetal maturation. In PNAE cases, 5mC was slightly greater than in controls. Images were taken at 200× magnification. DAB detection of antibody (brown) with hematoxylin counterstain (blue). The postconception age in weeks (w) is indicated for each panel. V = ventricle.

H3K36me3 exhibited less immunoreactivity ($p = 0.0054$) (Fig. 12). Decreases were observed among the epigenetics marks 5fC ($p = 0.0077$) and H3K36me3 ($p = 0.0058$) in the temporal lobe ependyma (Appendix S7).

## DISCUSSION

Epigenetic modifications play an important role in brain development, guiding the specification, differentiation, and maturation of neural progenitor cells (NPCs). NPCs in the mouse neural tube gain 5mC during specification, gain 5hmC during differentiation, and then lose 5mC in the later stages of maturation (Zhou, 2012). Similarly, in dentate granule neurons of the developing mouse hippocampus, a methylation gradient correlates with the outside-in pattern of neuronal maturation (Chen et al., 2013). Studies of rat and mouse brains have demonstrated associations between development and histone PTM changes (Cho et al., 2011; Hahn et al., 2013; Podobinska et al., 2017; Resendiz et al., 2014; Zhang et al., 2012). In order for stem cells to change from totipotency to pluripotency, active histone PTMs are present on gene promoters such as H3K27ac and H3K4me3. After NPCs begin to differentiate, many gene promoters are in a bivalent (poised state) with repressive histone PTMs such as H3K27me3 and activating histone PTMs such as H3K4me3 dually expressed, allowing them to rapidly turn on and off. When a brain cell is fully differentiated, repressive histone PTMs such as H3K27me3 are typically dominant (Podobinska et al., 2017). H3K4me2 and histone acetylation levels increase during differentiation of mouse NPCs (Resendiz et al., 2014; Zhang et al., 2012). Compared to NPCs, mature mouse cortical neurons are enriched in histone acetylation marks (Cho et al., 2011). Corresponding to findings in developing rodent brains, regulatory processes are reflected in our developmental expression graphs. For example, in hippocampal CA1 neurons, which can be identified without ambiguity, H3K27me3 (repressive) demonstrates a gradual increase during the fetal period (differentiation), followed by a gradual decrease during infancy. In contrast, H3K27ac (activating) demonstrated a gradual increase during infancy. These findings suggest that human hippocampal neurons have not reached genetic maturity in infancy, which is entirely consistent with observations that neuron size

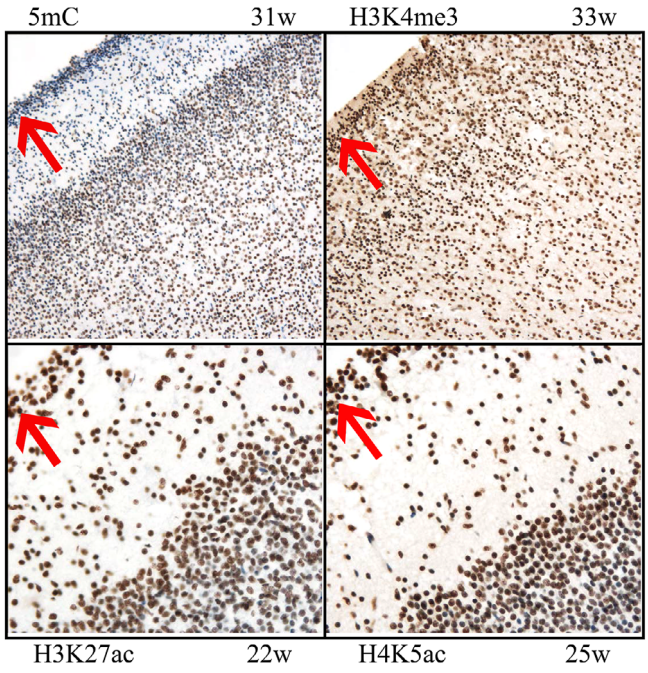


**Fig. 8.** Photomicrographs showing immunoreactivity for 4 epigenetic marks at the surface of temporal neocortex from normal human fetuses. The narrow band of immature marginal zone cells (red arrows) is positive for H3K4me3, H3K27ac, and H4K5ac, and negative for 5mC. Cells in deeper, more differentiated, layers of the cortex show mixed immunoreactivity. Images were taken at 20× (upper panels) and 200× (lower panels) magnifications. DAB detection of antibody (brown) with hematoxylin counterstain (blue). The gestational age in weeks (w) is indicated in each panel.

increases between 9 months and 16 years (Arnold and Trojanowski, 1996) and that synaptophysin accumulates in the CA1 sector throughout childhood and teenage years (Eastwood et al., 2006). However, because these immunohistochemical methods detect global (i.e., the average of 1,000s of gene loci) changes, we cannot infer specific functional changes with respect to any particular gene.

The VZ and SVZ, which collectively form the germinal matrix, in simplest terms give rise to glutamatergic and GABAergic interneurons, respectively (Adle-Biassette et al., 2018; ten Donkelaar, 2000). The SVZ also gives rise to precursors of astrocytes and oligodendrocytes. The size and proliferative activity within the SVZ peak between 20 and 26 weeks of gestation (Del Bigio, 2011), followed by rapid involution to 30 to 32 weeks and more gradual disappearance thereafter (Arshad et al., 2016). The proliferation peak in the temporal lobe is earlier (M. R. Del Bigio; unpublished findings). Our graphs of epigenetic PTMs suggest global increases in SVZ cell expression of H3K4me3, H3K9ac, and H4K5ac (which are all associated with active gene transcription) around the time of involution prior to 34 weeks gestation when the cells are leaving the proliferative stage. In the VZ of midgestation human fetuses studied here, PNAE was associated with reduced H4K12ac. However, in the SVZ no significant changes were observed. Ethanol has profound effects on the on survival and proliferation of NPCs (Boschen and Klintsova, 2017; Resendiz et al., 2014; Smith et al., 2014; Wilhelm and Guizzetti, 2016). This toxicity could account for the microcephaly in FASD (De La Monte and Kril, 2014; Jarmasz et al., 2017).

Among CA1 neurons of the fetal hippocampus, PNAE was associated with reduced immunoreactivity for 5mC, which is typically a gene transcription silencer. Within temporal cortex and hippocampus of young infants, we observed differential expression of several epigenetic marks in association with PNAE. The affected histone marks all play a role in active gene transcription. In experimental animals, most in utero and postnatal alcohol exposures caused a decrease in DNA methylation, a decrease in histone methylation, and an increase in histone acetylation (Chater-Diehl et al., 2017; Laufer et al., 2017; Lussier et al., 2017). These are in partial alignment with our results.

Because rodent brains are relatively immature at birth, many experiments use early postnatal alcohol administration to model late gestation human in utero exposure. Hippocampal and neocortical tissue from mice and rats that received alcohol during postnatal days 1 to 11 had increases in global DNA methylation, H3K4me3, H3K9me2, H3K27me2, and H3K27me3 (Chater-Diehl et al., 2016; Otero et al., 2012; Subbanna et al., 2013, 2014) and decreases in H3K9me2 and H3K27me2 (Subbanna et al., 2013). These results do not coincide with our findings. Discrepancies may be due to brain-specific interspecies differences or the absence of the maternal influences (i.e., maternal and placental metabolism) in the postnatal rodent experiments (Burd et al., 2007). In 1 recent study, mice were injected with ethanol (2.5 g/kg) on postnatal day 7 and euthanized ~8 h later. Global DNA methylation was decreased in the hippocampus and the cortex of ethanol-treated mice when compared to saline-treated mice (Nagre et al., 2015). This correlates with our findings in early fetuses despite the use of different methods. We must point out, however, that we do not know the interval between PNAE and fetal death.

In the absence of overt morphologic abnormalities, we observed several changes in epigenetic marks among the mature ciliated ependymal cells in both human and macaque PNAE. H3K4me3, H3K9ac, and H3K27ac were significantly reduced in humans, while 5fC and H3K36me3 were significantly reduced in macaques. The ependyma serves several functions including provision of a barrier between cerebrospinal fluid (CSF) and brain extracellular space, facilitating movement of signaling molecules in the CSF, and providing a niche for mature brain subventricular zone (stem) cells (Del Bigio, 2010; Ohata and Alvarez-Buylla, 2016). Little is known about epigenetic regulation in the mature ependymal layer. It is worth noting that, although none of the human cases studied here were hydrocephalic, hydrocephalus due to aqueduct stenosis was one of the more frequent malformations encountered in our PNAE/FASD autopsy study (Jarmasz et al., 2017). Integrity of the ependymal lining along the cerebral aqueduct is necessary for maintaining patency (Sival et al., 2011). We must consider the

**Table 4.** Statistically significant results for human control and PNAE pairings ($n$ = 18 pairs)

| | VZ | | SVZ | | Temporal cortex | | | | White matter | | | |
|---|---|---|---|---|---|---|---|---|---|---|---|---|
| | 21 to 25 PC weeks | 31 to 34 PC weeks | 21 to 25 PC weeks | 31 to 34 PC weeks | Early fetus | Late fetus | Young infant | Infant | Early fetus | Late fetus | Young infant | Infant |
| 5mC | ↓ $p$ = 0.4825 | ↓ $p$ = 0.9195 | ↓ $p$ = 0.2254 | ↑ $p$ = 0.0955 | ↓ $p$ = 0.1835 | ↓ $p$ = 0.1939 | ↓ $p$ = 0.0925 | ↓ $p$ = 0.6156 | ↓ $p$ = 0.1917 | ↓ $p$ = 0.5932 | ↓ $p$ = 0.4226 | ↑ $p$ = 0.8020 |
| 5hmC | ↓ $p$ = 0.5616 | ↑ $p$ = 0.4226 | ↑ $p$ = 0.4226 | n/a | ↑ $p$ = 0.3206 | ↓ $p$ = 0.5492 | ↓ $p$ = 0.1885 | ↓ $p$ = 0.5736 | ↓ $p$ = 0.4226 | ↑ $p$ = 0.6509 | – $p$ = 1.0 | ↓ $p$ = 0.4557 |
| 5fC | n/a | ↑ $p$ = 0.3103 | n/a | ↑ $p$ = 0.5470 | n/a | ↑ $p$ = 0.5367 | ↑ $p$ = 0.6889 | ↓ $p$ = 0.5903 | ↓ $p$ = 0.5000 | ↓ $p$ = 0.6810 | ↓ $p$ = 0.6352 | ↓ $p$ = 0.6560 |
| 5cac | ↓ $p$ = 0.7418 | ↑ $p$ = 0.2254 | ↓ $p$ = 0.8995 | ↓ $p$ = 0.0942 | ↓ $p$ = 0.5000 | ↓ $p$ = 0.4950 | ↑ $p$ = 0.6838 | ↓ $p$ = 0.9296 | ↓ $p$ = 0.5000 | ↓ $p$ = 0.2754 | ↑ $p$ = 0.4097 | ↓ $p$ = 0.5000 |
| H3K4me3 | ↓ $p$ = 0.7479 | – $p$ = 1.0 | ↑ $p$ = 0.8727 | ↓ $p$ = 0.2601 | ↑ $p$ = 0.8600 | ↓ $p$ = 0.4702 | *↓ $p$ = 0.0714* | ↓ $p$ = 0.4226 | ↑ $p$ = 0.8164 | ↓ $p$ = 0.7595 | ↓ $p$ = 0.5799 | *↓ $p$ = 0.0572* |
| H3K27me3 | ↓ $p$ = 0.4226 | ↑ $p$ = 0.4226 | ↑ $p$ = 0.4226 | ↑ $p$ = 0.1660 | ↓ $p$ = 0.5286 | ↓ $p$ = 0.7595 | ↓ $p$ = 0.1086 | ↑ $p$ = 0.8593 | ↓ $p$ = 0.4226 | ↑ $p$ = 0.8925 | ↓ $p$ = 0.2495 | n/a |
| H3K36me3 | ↓ $p$ = 0.6815 | ↑ $p$ = 0.1588 | ↑ $p$ = 0.3206 | ↑ $p$ = 0.1066 | ↑ $p$ = 0.7060 | ↑ $p$ = 0.5465 | ↓ $p$ = 0.2044 | ↑ $p$ = 0.7418 | ↓ $p$ = 0.9388 | ↓ $p$ = 0.8084 | ↓ $p$ = 0.2149 | ↓ $p$ = 0.2522 |
| H3K9ac | ↓ $p$ = 0.5070 | ↑ $p$ = 0.0955 | ↑ $p$ = 0.6667 | ↑ $p$ = 0.0942 | *↓ $p$ = 0.0572* | ↑ $p$ = 0.5401 | **↓ $p$ = 0.0202** | ↓ $p$ = 0.4226 | **↓ $p$ = 0.0377** | ↓ $p$ = 0.6350 | ↑ $p$ = 0.9553 | ↓ $p$ = 0.3832 |
| H3K14ac | ↓ $p$ = 0.8379 | ↑ $p$ = 0.4226 | ↓ $p$ = 0.5509 | ↑ $p$ = 0.2079 | ↓ $p$ = 0.7952 | ↓ $p$ = 0.5304 | ↑ $p$ = 0.2412 | ↓ $p$ = 0.5979 | ↓ $p$ = 0.2578 | ↑ $p$ = 0.5082 | – $p$ = 1.0 | ↓ $p$ = 0.4778 |
| H3K27ac | ↓ $p$ = 0.8520 | ↑ $p$ = 0.2811 | ↑ $p$ = 0.8845 | ↑ $p$ = 0.0904 | ↓ $p$ = 0.7240 | ↓ $p$ = 0.7295 | **↓ $p$ = 0.0229** | ↑ $p$ = 0.7204 | ↓ $p$ = 0.7852 | ↑ $p$ = 0.4226 | ↓ $p$ = 0.8528 | ↑ $p$ = 0.5624 |
| H4K5ac | ↑ $p$ = 0.1917 | ↓ $p$ = 0.8845 | ↑ $p$ = 0.4928 | ↑ $p$ = 0.9139 | ↑ $p$ = 0.7072 | ↑ $p$ = 0.8240 | ↓ $p$ = 0.1835 | ↑ $p$ = 0.8556 | ↓ $p$ = 0.4522 | ↓ $p$ = 0.1836 | – $p$ = 1.0 | ↑ $p$ = 0.9423 |
| H4K12ac | **↓ $p$ = 0.0039** | ↑ $p$ = 0.2567 | ↑ $p$ = 0.6891 | ↑ $p$ = 0.4380 | ↑ $p$ = 0.1869 | ↑ $p$ = 0.6971 | ↓ $p$ = 0.7295 | ↑ $p$ = 0.2254 | ↓ $p$ = 0.6035 | – $p$ = 1.0 | n/a | ↑ $p$ = 0.6657 |
| H4K16ac | ↓ $p$ = 0.1994 | ↑ $p$ = 0.1660 | ↓ $p$ = 0.0815 | ↑ $p$ = 0.8075 | ↓ $p$ = 0.2222 | ↓ $p$ = 0.4119 | ↓ $p$ = 0.1529 | ↑ $p$ = 0.3949 | ↓ $p$ = 0.1835 | *↓ $p$ = 0.0661* | ↓ $p$ = 0.1359 | ↑ $p$ = 0.6560 |

| | Temporal ependyma | | | | Dentate gyrus | | | | CA1 | | | |
|---|---|---|---|---|---|---|---|---|---|---|---|---|
| | Early fetus | Late fetus | Young infant | Infant | Early fetus | Late fetus | Young infant | Infant | Early fetus | Late fetus | Young infant | Infant |
| 5mC | ↓ $p$ = 0.4326 | ↑ $p$ = 0.7202 | ↓ $p$ = 0.7209 | ↑ $p$ = 0.6914 | ↓ $p$ = 0.4226 | ↓ $p$ = 0.8077 | – $p$ = 1.0 | ↑ $p$ = 0.1917 | **↓ $p$ = 0.0198** | ↓ $p$ = 0.7717 | ↓ $p$ = 0.4226 | ↓ $p$ = 0.4226 |
| 5hmC | ↑ $p$ = 0.6667 | ↓ $p$ = 0.4296 | ↓ $p$ = 0.2601 | ↓ $p$ = 0.7234 | – $p$ = 1.0 | ↓ $p$ = 0.6349 | ↑ $p$ = 0.8845 | ↓ $p$ = 0.7779 | ↑ $p$ = 0.2697 | ↓ $p$ = 0.8399 | ↓ $p$ = 0.4226 | n/a |
| 5fC | n/a | ↑ $p$ = 0.2413 | ↑ $p$ = 0.0872 | ↑ $p$ = 0.4208 | n/a | ↑ $p$ = 0.3910 | ↓ $p$ = 0.9649 | ↑ $p$ = 0.2780 | n/a | ↑ $p$ = 0.7090 | ↓ $p$ = 0.9448 | ↑ $p$ = 0.5529 |
| 5cac | ↓ $p$ = 0.5000 | ↑ $p$ = 0.2941 | ↓ $p$ = 0.8248 | ↓ $p$ = 0.5000 | ↓ $p$ = 0.5000 | ↓ $p$ = 0.2444 | ↑ $p$ = 0.4611 | ↓ $p$ = 0.9097 | ↑ $p$ = 0.5000 | ↑ $p$ = 0.7045 | ↑ $p$ = 0.4720 | ↓ $p$ = 0.5000 |
| H3K4me3 | **↓ $p$ = 0.0234** | ↑ $p$ = 0.1856 | ↓ $p$ = 0.5112 | ↓ $p$ = 0.3745 | ↓ $p$ = 0.5228 | ↓ $p$ = 0.6140 | ↓ $p$ = 0.1675 | ↓ $p$ = 0.5492 | ↓ $p$ = 0.6278 | ↓ $p$ = 0.6638 | ↓ $p$ = 0.0797 | ↑ $p$ = 0.6621 |
| H3K27me3 | ↓ $p$ = 0.7418 | ↑ $p$ = 0.2620 | ↑ $p$ = 0.9388 | ↓ $p$ = 0.8725 | – $p$ = 1.0 | ↓ $p$ = 0.7707 | ↓ $p$ = 0.1849 | ↓ $p$ = 0.2379 | ↓ $p$ = 0.8740 | ↓ $p$ = 0.8614 | ↓ $p$ = 0.1835 | ↑ $p$ = 0.8870 |
| H3K36me3 | ↓ $p$ = 0.1839 | – $p$ = 1.0 | ↑ $p$ = 0.1835 | ↑ $p$ = 0.4078 | ↓ $p$ = 0.9261 | ↓ $p$ = 0.9299 | ↑ $p$ = 0.1835 | ↑ $p$ = 0.1835 | ↓ $p$ = 0.4226 | ↓ $p$ = 0.4740 | ↓ $p$ = 0.4226 | ↑ $p$ = 0.2254 |
| H3K9ac | **↓ $p$ = 0.0198** | ↑ $p$ = 0.4194 | ↑ $p$ = 0.2379 | ↑ $p$ = 0.9521 | ↓ $p$ = 0.9374 | ↑ $p$ = 0.5913 | **↑ $p$ = 0.0352** | ↓ $p$ = 0.6695 | ↓ $p$ = 0.3681 | ↑ $p$ = 0.8854 | ↑ $p$ = 0.4226 | ↓ $p$ = 0.3719 |
| H3K14ac | ↓ $p$ = 0.1638 | ↓ $p$ = 0.8907 | ↓ $p$ = 0.2589 | ↓ $p$ = 0.0979 | ↓ $p$ = 0.2952 | ↓ $p$ = 0.6584 | ↓ $p$ = 0.6613 | ↓ $p$ = 0.4776 | ↓ $p$ = 0.5000 | ↑ $p$ = 0.8052 | ↓ $p$ = 0.8259 | ↓ $p$ = 0.2057 |
| H3K27ac | **↓ $p$ = 0.0142** | ↓ $p$ = 0.7234 | ↑ $p$ = 0.7852 | ↑ $p$ = 0.1994 | ↓ $p$ = 0.3232 | ↑ $p$ = 0.4226 | ↑ $p$ = 0.4341 | ↑ $p$ = 0.2324 | ↓ $p$ = 0.7538 | ↑ $p$ = 0.4226 | ↑ $p$ = 0.8706 | **↓ $p$ = 0.0414** |
| H4K5ac | ↓ $p$ = 0.2999 | ↓ $p$ = 0.5908 | ↓ $p$ = 0.4226 | ↑ $p$ = 0.2048 | ↓ $p$ = 0.1096 | ↑ $p$ = 0.2152 | ↓ $p$ = 0.2999 | ↑ $p$ = 0.5000 | – $p$ = 1.0 | ↑ $p$ = 0.1817 | ↓ $p$ = 0.5112 | n/a |
| H4K12ac | ↓ $p$ = 0.1038 | ↑ $p$ = 0.9087 | ↓ $p$ = 0.4226 | ↑ $p$ = 0.4226 | ↑ $p$ = 0.6129 | ↑ $p$ = 0.1826 | ↑ $p$ = 0.4226 | – $p$ = 1.0 | ↓ $p$ = 0.2044 | n/a | n/a | ↑ $p$ = 0.4226 |
| H4K16ac | ↓ $p$ = 0.4226 | ↑ $p$ = 0.4766 | ↓ $p$ = 0.1828 | ↓ $p$ = 0.6392 | ↓ $p$ = 0.4226 | ↑ $p$ = 0.8628 | **↓ $p$ = 0.0339** | ↓ $p$ = 0.5000 | ↓ $p$ = 0.1460 | ↓ $p$ = 0.6702 | ↓ $p$ = 0.4460 | n/a |

Early fetus = 21 to 25 weeks postconception (PC); late fetus = 31 to 40 weeks PC; early infant = 43 to 48.5 weeks PC; infant = 53 to 70.5 weeks PC.
Up and down arrows represent the direction of change; a dash represents no change.
n/a represents comparisons that had low ranked values and too few comparisons to generate a valid $p$ value.
Two-tailed $p$ values are significant at $p < 0.05$ and are in bold; 1-tailed $p$ values significant at $p < 0.05$ showing a trend are italic and underlined.

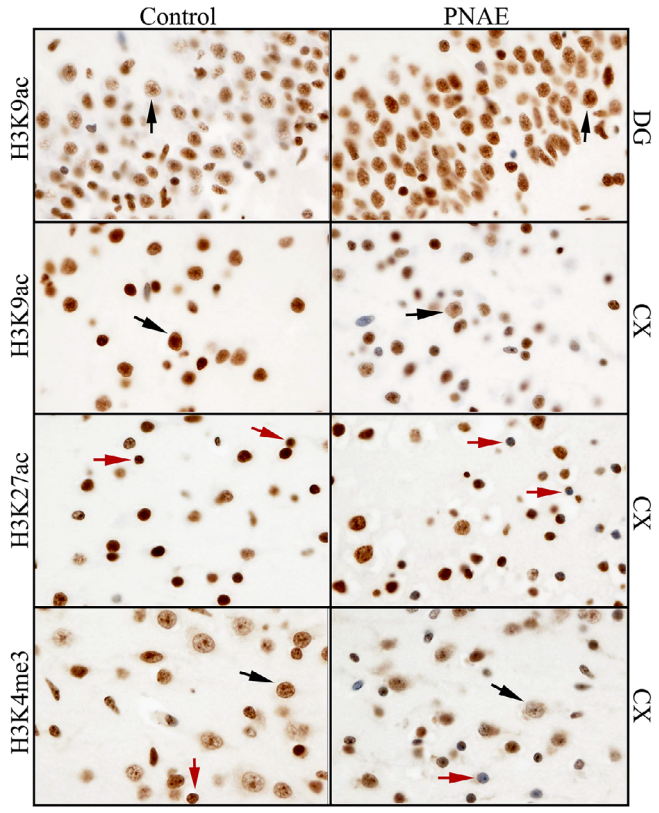


**Fig. 9.** Photomicrographs showing immunoreactivity for histone acetylation and methylation marks in human control and PNAE dentate gyrus (DG) and temporal neocortex. In the DG of young infants (43 weeks postconception), granular neurons of PNAE cases had greater immunoreactivity for H3K9ac than controls ($p = 0.0352$). In the temporal cortex of young infant PNAE cases, large neurons (black arrows) had less intense immunoreactivity than controls for histone marks H3K9ac ($p = 0.0202$) and H3K27ac ($p = 0.0229$). Reduced immunoreactivity was also apparent in small round nuclei (presumably oligodendrocytes; red arrows). Images were taken at 200× magnification. DAB detection of antibody (brown) with hematoxylin counterstain (blue).

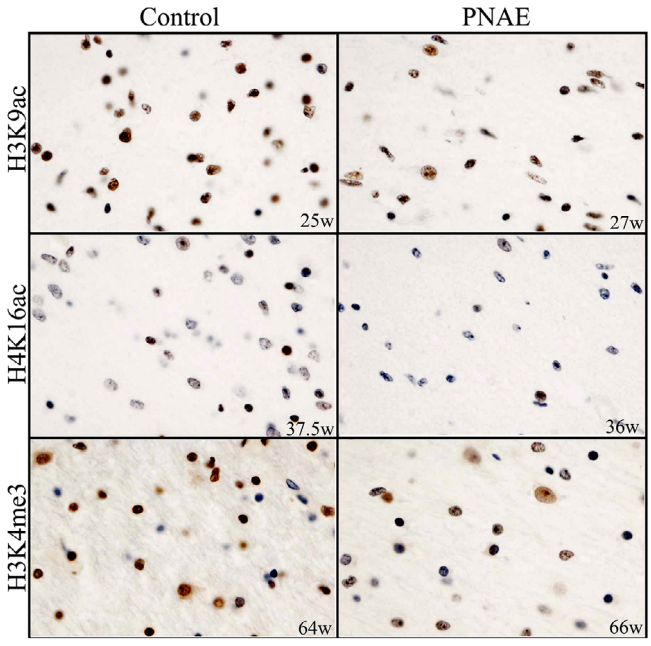


**Fig. 10.** Photomicrographs showing immunoreactivity for epigenetic marks in human control and PNAE white matter. Compared to controls, H3K9ac was lower in early fetal (21 to 25 weeks) PNAE ($p = 0.0377$). Both H4K16ac and H3K4me3 also tended to be lower ($p = 0.0661$ and $p = 0.0572$, respectively) in the late fetal (31 to 40 weeks) and infant (53 to 70.5 weeks) groups. These global decreases in immunoreactivity did not appear to be cell morphology specific. The postconception age in weeks (w) is indicated for each panel. Images were taken at 200× magnification. DAB detection of antibody (brown) with hematoxylin counterstain (blue).

possibility that PNAE-associated epigenetic changes might adversely affect the function of ependymal cells, which in turn could alter the health of the subjacent NPCs.

Owing to the difficulty obtaining human specimens with documented history of PNAE, there are numerous limitations to our study. (i) Small sample sizes in heterogenous groups are subject to type II errors (i.e., failure to identify real differences). (ii) We calculated numerous nonindependent paired t-tests, which increases the risk for type I error. Hence, these data must be considered exploratory and the reported $p$ values should be viewed with caution. (iii) None of the cases had a comprehensive genetic (i.e., gene mutation) analysis, so we cannot be certain that abnormalities attributed to PNAE are, in fact, related to an unrecognized genetic disorder (Zarrei et al., 2018). We previously described many complex abnormalities and confounding factors in the autopsy cohort of PNAE/FASD cases (Jarmasz et al., 2017). Here, we avoided cases with severe malformations and attempted to restrict the analysis to brains of small size (micrencephaly). (iv) Hypoxic-ischemic stress frequently occurs prior to in utero death of fetuses; oxidative stress due to placental insufficiency could mask epigenetic changes caused by PNAE (Brocardo et al., 2011). In a largely overlapping cohort of human fetal and infant brains with a history of PNAE, we found immunohistochemical evidence for oxidative changes in the DNA and lipids of stillborn fetus brains, but there were no differences between controls and PNAE cases (Appendix S8). (v) We showed in a previous study (Jarmasz et al., 2019) that some histone acetylation marks diminish with increasing PMD. This necessitated the use of PMD time as an additional factor to be controlled, which in turn narrowed options for control cases. (vi) The unavoidably imprecise history of alcohol use (timing and quantity) during the pregnancy (Jarmasz et al., 2017) could explain the lack of consistent changes among epigenetic marks. Precisely timed studies in pregnant mice have shown, for example, that the offspring have different phenotypes when PNAE occurs on gestational day 7 compared with day 8 (Sulik, 2005). Extremely high doses at earlier stages can lead to more severe abnormalities such as neural tube defects (Hunter et al., 1994).

To compensate for the limitations of the human samples, we included a parallel analysis of macaque monkey binge PNAE brain samples. However, even within the controlled experiment, variable phenotypic outcomes were encountered (Clarren et al., 1990; Sheller et al., 1988). There are several possible reasons why our human and macaque results did

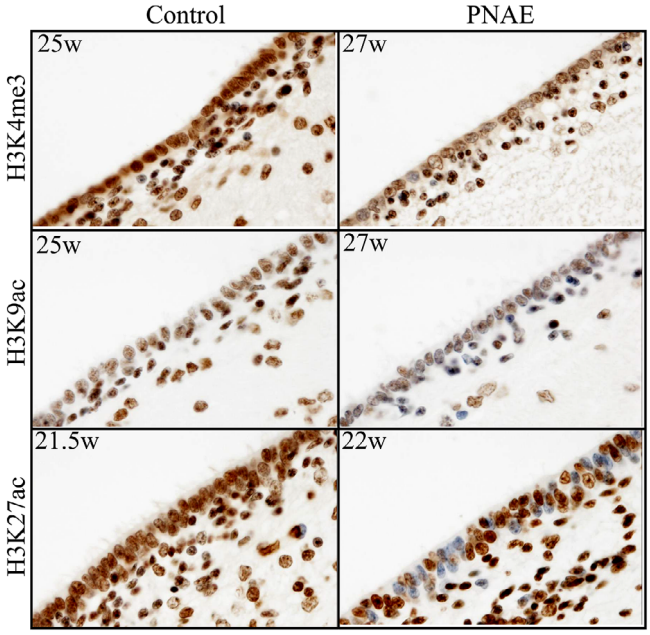


**Fig. 11.** Photomicrographs showing immunoreactivity for epigenetic marks in ependymal cells lining the temporal horn of human control and PNAE cases. Compared to controls, the intensities of H3K4me3 ($p = 0.0234$) and H3K9ac ($p = 0.0198$) were significantly lower in the early fetal age group (21 to 25 weeks). For H3K27ac, the proportion of positive cells was lower ($p = 0.0142$). The postconception age in weeks (w) is indicated for each panel. Images were taken at 200× magnification. DAB detection of antibody (brown) with hematoxylin counterstain (blue).

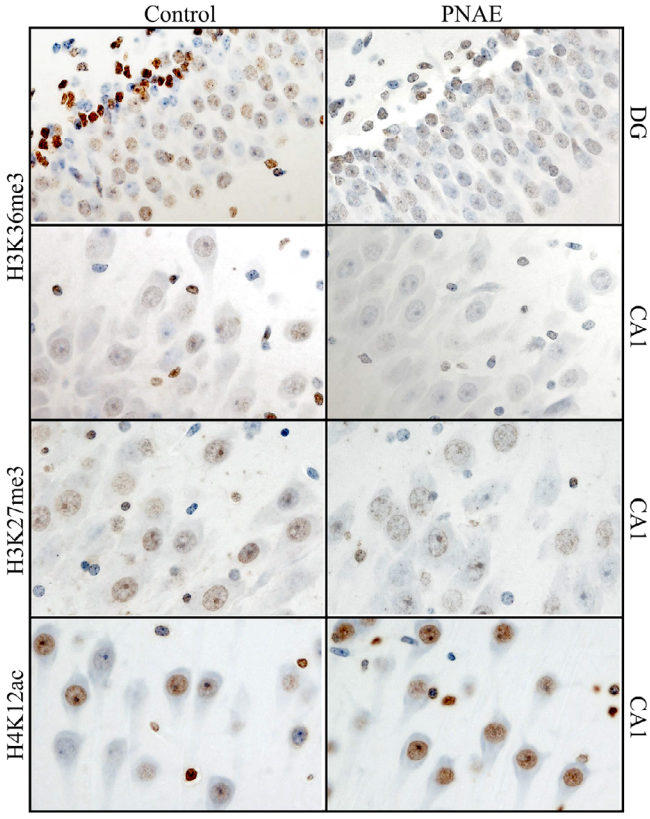


**Fig. 12.** Photomicrographs showing immunoreactivity for epigenetic marks in ~6-month-old control and PNAE macaque hippocampal neurons. H3K36me3 was significantly lower in the immature cells of the dentate gyrus adjacent to the cornu ammonis CA4 region ($p = 0.0054$). Among CA1 neurons, the proportions of neurons immunoreactive for H3K9ac ($p = 0.0253$) and H3K27me3 ($p = 0.0146$) were reduced in PNAE, while the proportion of H4K12ac-positive cells in PNAE cases was increased ($p = 0.0445$). Images were taken at 400× magnifications. DAB detection of antibody (brown) with hematoxylin counterstain (blue).

not correspond. The monkey brain sections required slightly different immunohistochemical techniques and often had inconsistent labeling, likely related to prolonged fixation in formalin. The humans died from natural causes, which would often include some degree of hypoxia, and the monkeys died from anesthetic overdoses, which are unlikely to immediately cause changes in epigenetics (Ju et al., 2016; Mori et al., 2014; Pekny et al., 2014). Although the monkeys survived a similar postnatal duration (6 months), in comparative developmental terms, they are approximately equivalent to 2.7- to 3.5-year-old humans (http://translatingtime.org/translate). In addition, a recent study documented transcriptional differences between the brains of humans and rhesus macaques in prenatal, early postnatal, and adult

**Table 5.** Statistically significant results for macaque control and PNAE pairings

| Epigenetic mark | Ependyma | Temporal cortex | White matter | Dentate gyrus | CA1 neurons |
|---|---|---|---|---|---|
| 5mC | ↑ $p = 0.8531$ | ↓ $p = 0.0821$ | ↓ $p = 0.5161$ | ↑ $p = 0.4601$ | ↓ $p = 0.7808$ |
| 5hmC | ↓ $p = 0.1982$ | ↓ $p = 0.3367$ | ↑ $p = 0.3547$ | ↓ $p = 0.1570$ | ↓ $p = 0.0840$ |
| 5fC | ↓ $\mathbf{p = 0.0077}$ | ↑ $p = 0.5751$ | ↓ $p = 0.1961$ | ↓ $p = 0.3800$ | ↓ $p = 0.1024$ |
| 5caC | ↓ $\underline{p = 0.0210}$ | ↑ $p = 0.5080$ | ↓ $p = 0.1138$ | ↓ $p = 0.5192$ | – $p = 1.0$[a] |
| H3K4me3 | ↓ $p = 0.5614$ | ↓ $p = 0.6435$ | ↓ $p = 0.4621$ | ↑ $p = 0.5541$ | ↑ $p = 0.6423$ |
| H3K9me2/K9me3 | ↓ $p = 0.0910$ | $p = 0.9004$ | ↓ $p = 0.7074$ | ↑ $p = 0.1898$ | ↑ $p = 0.7266$ |
| H3K27me3 | ↓ $p = 0.1113$ | ↓ $p = 0.6873$ | ↓ $p = 0.3547$ | ↓ $p = 0.2667$ | ↓ $\underline{p = 0.0146}$ |
| H3K36me3 | ↓ $\mathbf{p = 0.0058}$ | ↓ $\underline{p = 0.0112}$ | ↓ $p = 0.1395$ | ↓ $\mathbf{p = 0.0054}$ | ↓ $\underline{p = 0.0253}$ |
| H3K9ac | ↓ $\underline{p = 0.0427}$ | ↓ $p = 0.9228$[a] | ↓ $p = 0.2278$ | ↓ $p = 0.9261$ | ↓ $p = 0.2733$[a] |
| H3K27ac | ↓ $p = 0.3052$ | ↓ $p = 0.4388$ | ↑ $p = 0.3501$ | ↑ $p = 0.7010$ | ↓ $p = 0.8500$ |
| H4K5ac | ↑ $p = 0.3547$ | ↑ $p = 0.6620$ | ↓ $p = 0.5787$ | ↑ $p = 0.1303$[a] | ↑ $p = 0.3613$ |
| H4K12ac | ↓ $p = 0.9247$ | ↓ $p = 0.1386$ | ↑ $p = 0.7813$ | ↑ $p = 0.9155$ | ↑ $\underline{p = 0.0445}$[a] |

Bolded $p$ values represent statistical significance at $p < 0.05$ after Benjamini–Hochberg correction at a false discovery rate of 0.1. $p$ Values significant at $p < 0.05$ but failed Benjamini–Hochberg correction represent a trend and are italic and underlined.

↓—decreased in PNAE ($n = 6$) relative to control ($n = 5$); ↑—increased in PNAE ($n = 6$) relative to control ($n = 5$); "–" represents no change in PNAE ($n = 6$) relative to control ($n = 5$).

[a]Minimal immunoreactivity.

stages of life. The postconception day 60 macaque specimens were fairly closely aligned with postconception day 102 to 115 human samples, while 2- to 7-year-old macaques aligned with adolescent and adult human samples. This indicates a protracted development of the brain in humans in comparison with rhesus macaques at the level of gene transcription, which is an epigenetically driven process (Zhu et al., 2018).

A major target in FASD research is identification of a DNA methylation pattern sufficiently characteristic to be used as a biomarker for early diagnosis in living children. This usually relies on whole genome methylation analysis of DNA extracted from leukocytes or buccal epithelium cells. In buccal cells from 12 males with FASD (3 to 6 years), 269 differentially methylated cytosine–phosphate–guanines (CpGs) were identified (Laufer et al., 2015). In buccal cells from 110 FASD and 96 control children (5 to 18 years), differentially methylated CpGs were found in 403 genes, many of which are related to neurons and brain diseases (e.g., autism, epilepsy, substance abuse; Portales-Casamar et al., 2016). In a separate validation cohort of 24 FASD and 24 control children (ages 3.5 to 18 years), 82 hypermethylated and 79 hypomethylated genes were detected, some the same as in the previous study (Lussier et al., 2018). The extent to which gene-specific methylation changes in buccal epithelial cells reflects upon global methylation in the nuclei of brain neurons is unknown.

In summary, we showed a variety of global epigenetic changes in brain cell nuclei of human fetuses and infants with a history of PNAE. These partially align with experimental PNAE studies in rodents. However, rapid developmental changes in the expression of specific DNA cytosine modifications and histone PTMs across ages, as well as environmental influences, make it difficult to translate observations in rodents to findings in humans. In general, our exploratory findings support the broad hypothesis that DNA and histone epigenetic changes occur in PNAE. These changes might contribute to the abnormalities in brain development that are associated with FASD. Future work will include detailed cell type analysis (e.g., with double-label immunofluorescence) to confirm specific cell populations affected by PNAE, in particular the heterogenous progenitor cells in the SVZ and the multiple cell types in the cerebral cortex. Eventually, we hope to correlate these global changes with gene-specific modifications in brain and perhaps in accessible nonneural tissues.

## ACKNOWLEDGMENTS

We thank Susan Janeczko and Diane Legarta for technical assistance.

## FUNDING

This work was funded by a grant from the Canadian Institutes of Health Research (CIHR, grant # TEC—128094) and a grant from Canada Israel International Fetal Alcohol Consortium (CIIFAC). Dr. Del Bigio and Dr. Davie are supported by the Canada Research Chairs program. Ms. Jarmasz was funded by the Graduate Enhancement of Tri-Council Stipends (GETS) through the University of Manitoba, and by a scholarship from the Liquor and Gaming Authority of Manitoba. The original Macaque study was supported by USPHS Grants AA05616, RR00166, and HD02274.

## CONFLICT OF INTEREST

The authors declare that they have no conflict of interest.

## RESEARCH INVOLVING HUMAN PARTICIPANTS AND/OR ANIMALS

All applicable international, national, and/or institutional guidelines for the care and use of animals were followed. For the human study, ethics approval was obtained from the Research Ethics Board at the University of Manitoba (#HS1311 – H2011:213). The Macaque Project was performed in the Infant Primate Research Laboratory (jointly operated by the University of Washington Regional Primate Research Center and the Child Development and Mental Retardation Center of the University of Washington Center on Human Development & Disability) in compliance with University of Washington Administrative Policy for the humane treatment of animals used in research.

## INFORMED CONSENT

The tissues analyzed were selected retrospectively; the Research Ethics Board agreed that the potential for emotional harm to parents contacted about deceased children exceeded the risks of discovery about important unknown pathology.

## AUTHORS' CONTRIBUTIONS

JSJ conducted almost all the research, put almost all results together, and wrote the manuscript. HS performed some of the Macaque immunostaining and imaging. DB analyzed oxidative changes in brain tissue and reprocessed the monkey brain tissue. SJA and SKC provided the Macaque brain samples and contributed to the discussion and final review of the manuscript. JRD provided guidance over the selection of markers and contributed to the discussion and final review of the manuscript discussion. MRD planned the project, provided financial support, effectuated the statistical analysis, and finalized the manuscript.

## REFERENCES

Adle-Biassette H, Harding B, Golden J (Eds.) (2018) Developmental Neuropathology, 2nd ed. John Wiley & Sons Ltd, Hoboken, NJ.

Arnold SE, Trojanowski JQ (1996) Human fetal hippocampal development: and neuronal morphologic features. J Comp Neurol 367:274–292.

Arshad A, Vose LR, Vinukonda G, Hu F, Yoshikawa K, Csiszar A, Brumberg JC, Ballabh P (2016) Extended production of cortical interneurons into the third trimester of human gestation. Cereb Cortex 26:2242–2256.

Bender R, Lange S (2001) Adjusting for multiple testing-when and how? J Clin Epidemiol 54:343–349.

Benjamini Y, Hochberg Y (1995) Controlling the false discovery rate: a practical and powerful approach to multiple testing. J R Soc Ser B 57:289–300.

Bonthius DJ, Bonthius NE, Napper RM, Astley SJ, Clarren SK, West JR (1996) Purkinje cell deficits in nonhuman primates following weekly exposure to ethanol during gestation. Teratology 53:230–236.

Boschen KE, Klintsova AY (2017) Disruptions to hippocampal adult neurogenesis in rodent models of fetal alcohol spectrum disorders. Neurogenesis 4:e1324259.

Brocardo PS, Gil-Mohapel J, Christie BR (2011) The role of oxidative stress in fetal alcohol spectrum disorders. Brain Res Rev 67:209–225.

Burd L, Roberts D, Olson M, Odendaal H (2007) Ethanol and the placenta: a review. J Matern Neonatal Med 20:361–375.

Carson G, Cox LV, Crane J, Croteau P, Graves L, Kluka S, Koren G, Martel M-J, Midmer D, Nulman I, Poole N, Senikas V, Wood R, Society of Obstetricians and Gynaecologists of Canada (2010) Alcohol use and pregnancy consensus clinical guidelines. J Obstet Gynaecol Canada 32:S1–S31.

Chater-Diehl EJ, Laufer BI, Castellani CA, Alberry BL, Singh SM (2016) Alteration of gene expression, DNA methylation, and histone methylation in free radical scavenging networks in adult mouse hippocampus following fetal alcohol exposure. PLoS One 11:1–25.

Chater-Diehl EJ, Laufer BI, Singh SM (2017) Changes to histone modifications following prenatal alcohol exposure: an emerging picture. Alcohol 60:41–52.

Chen Y, Ozturk NC, Zhou FC (2013) DNA methylation program in developing hippocampus and its alteration by alcohol. PLoS One 8:1–11.

Cho B, Kim HJ, Kim H, Sun W (2011) Changes in the histone acetylation patterns during the development of the nervous system. Exp Neurobiol 20:81.

Cipriani V, Quartilho A, Bunce C, Freemantle N, Doré CJ (2015) Ophthalmic statistics note 7: multiple hypothesis testing-to adjust or not to adjust. Br J Ophthalmol 99:1155–1157.

Clarren SK, Astley SJ, Bowden DM (1988) Physical anomalies and developmental delays in nonhuman primate infants exposed to weekly doses of ethanol during gestation. Teratology 37:561–569.

Clarren SK, Astley SJ, Bowden DM, Lai H, Milam AH, Rudeen PK, Shoemaker WJ (1990) Neuroanatomic and neurochemical abnormalities in non-human primate infants exposed to weekly doses of ethanol during gestation. Alcohol Clin Exp Res 14:674–683.

Clarren SK, Bowden DM, Astley SJ (1987) Pregnancy outcomes after weekly oral administration of ethanol during gestation in the pig-tailed macaque (*Macaca nemestrina*). Teratology 35:345–354.

Coskun V, Tsoa R, Sun YE (2012) Epigenetic regulation of stem cells differentiating along the neural lineage. Curr Opin Neurobiol 22:762–767.

Costa MR, Kessaris N, Richardson WD, Götz M, Hedin-Pereira C (2007) The marginal zone/layer I as a novel niche for neurogenesis and gliogenesis in developing cerebral cortex. J Neurosci 27:11376–11388.

De La Monte SM, Kril JJ (2014) Human alcohol-related neuropathology. Acta Neuropathol 127:71–90.

Dekaban AS (1978) Changes in brain weights during the span of human life: relation of brain weights to body heights and body weights. Ann Neurol 4:345–356.

Del Bigio MR (2010) Ependymal cells: biology and pathology. Acta Neuropathol 119:55–73.

Del Bigio MR (2011) Cell proliferation in human ganglionic eminence and suppression after prematurity-associated haemorrhage. Brain 134:1344–1361.

Donald KA, Eastman E, Howells FM, Adnams C, Riley EP, Woods RP, Narr KL, Stein DJ (2015) Neuroimaging effects of prenatal alcohol exposure on the developing human brain: a magnetic resonance imaging review. Acta Neuropsychiatr 27:251–269.

ten Donkelaar HJ (2000) Major events in the development of the forebrain. Eur J Morphol 38:301–308.

Eastwood SL, Weickert CS, Webster MJ, Herman MM, Kleinman JE, Harrison PJ (2006) Synaptophysin protein and mRNA expression in the human hippocampal formation from birth to old age. Hippocampus 16:645–654.

Feinberg AP (2018) The key role of epigenetics in human disease prevention and mitigation. N Engl J Med 378:1323–1334.

Hahn MA, Qiu R, Wu X, Li AX, Zhang H, Wang J, Jui J, Jin SG, Jiang Y, Pfeifer GP, Lu Q (2013) Dynamics of 5-Hydroxymethylcytosine and chromatin marks in mammalian neurogenesis. Cell Rep 3:291–300.

Hirabayashi Y, Gotoh Y (2010) Epigenetic control of neural precursor cell fate during development. Nat Rev Neurosci 11:377–388.

Hunter ES, Tugman JA, Sulik KK, Sadler TW (1994) Effects of short-term exposure to ethanol on mouse embryos in vitro. Toxicol In Vitro 8:413–421.

Jacobson SW, Jacobson JL, Molteno CD, Warton CMR, Wintermark P, Hoyme HE, De Jong G, Taylor P, Warton F, Lindinger NM, Carter RC, Dodge NC, Grant E, Warfield SK, Zöllei L, van der Kouwe AJW, Meintjes EM (2017) Heavy prenatal alcohol exposure is related to smaller corpus callosum in newborn MRI scans. Alcohol Clin Exp Res 41:965–975.

Jarmasz JS, Basalah DA, Chudley AE, Del Bigio MR (2017) Human brain abnormalities associated with prenatal alcohol exposure and fetal alcohol spectrum disorder. J Neuropathol Exp Neurol 76:813–833.

Jarmasz JS, Stirton H, Davie JR, Del Bigio MR (2019) DNA methylation and histone post-translational modification stability in post-mortem brain tissue. Clin Epigenetics 11:1–23.

Ju L, Jia M, Sun J, Sun X, Zhang H, Ji M, Yang J, Wang Z (2016) Hypermethylation of hippocampal synaptic plasticity-related genes is involved in neonatal sevoflurane exposure-induced cognitive impairments in rats. Neurotox Res 29:243–255.

Kigar SL, Auger AP (2013) Epigenetic mechanisms may underlie the aetiology of sex differences in mental health risk and resilience. J Neuroendocrinol 25:1141–1150.

Kundakovic M, Champagne FA (2015) Early-life experience, Epigenetics, and the developing brain. Neuropsychopharmacology 40:141–153.

Lange S, Probst C, Gmel G, Rehm J, Burd L, Popova S (2017) Global prevalence of fetal alcohol spectrum disorder among children and youth: a systematic review and meta-analysis. JAMA Pediatr 171:948–956.

Laufer BI, Chater-Diehl EJ, Kapalanga J, Singh SM (2017) Long-term alterations to DNA methylation as a biomarker of prenatal alcohol exposure: from mouse models to human children with fetal alcohol spectrum disorders. Alcohol 60:67–75.

Laufer BI, Kapalanga J, Castellani CA, Diehl EJ, Yan L, Singh SM (2015) Associative DNA methylation changes in children with prenatal alcohol exposure. Epigenomics 7:1259–1274.

Liu J, Moyon S, Hernandez M, Casaccia P (2016) Epigenetic control of oligodendrocyte development: adding new players to old keepers. Curr Opin Neurobiol 39:133–138.

Lussier AA, Morin AM, MacIsaac JL, Salmon J, Weinberg J, Reynolds JN, Pavlidis P, Chudley AE, Kobor MS (2018) DNA methylation as a predictor of fetal alcohol spectrum disorder. Clin Epigenetics 10:1–14.

Lussier AA, Weinberg J, Kobor MS (2017) Epigenetics studies of fetal alcohol spectrum disorder: where are we now? Epigenomics 9:291–311.

Menger Y, Bettscheider M, Murgatroyd C, Spengler D (2010) Sex differences in brain epigenetics. Epigenomics 2:807–821.

Moore EM, Migliorini R, Infante MA, Riley EP (2014) Fetal alcohol spectrum disorders: recent neuroimaging findings. Curr Dev Disord Rep 1:161–172.

Mori K, Iijima N, Higo S, Aikawa S, Matsuo I, Takumi K, Sakamoto A, Ozawa H (2014) Epigenetic suppression of mouse Per2 expression in the suprachiasmatic nucleus by the inhalational anesthetic, sevoflurane. PLoS One 9:e87319.

Nagre NN, Subbanna S, Shivakumar M, Psychoyos D, Basavarajappa BS (2015) CB1-receptor knockout neonatal mice are protected against ethanol-induced impairments of DNMT1, DNMT3A, and DNA methylation. J Neurochem 132:429–442.

Nardelli A, Lebel C, Rasmussen C, Andrew G, Beaulieu C (2011) Extensive deep gray matter volume reductions in children and adolescents with fetal alcohol spectrum disorders. Alcohol Clin Exp Res 35:1404–1417.

Norman AL, Crocker N, Mattson SN, Riley EP (2009) Neuroimaging and fetal alcohol spectrum disorders. Dev Disabil Res Rev 15:209–217.

Ohata S, Alvarez-Buylla A (2016) Planar organization of multiciliated Ependymal (E1) cells in the brain ventricular epithelium. Trends Neurosci 39:543–551.

Otero NKH, Thomas JD, Saski CA, Xia X, Kelly SJ (2012) Choline supplementation and DNA methylation in the hippocampus and prefrontal cortex of rats exposed to alcohol during development. Alcohol Clin Exp Res 36:1701–1709.

Pekny T, Andersson D, Wilhelmsson U, Pekna M, Pekny M (2014) Short general anaesthesia induces prolonged changes in gene expression in the mouse hippocampus. Acta Anaesthesiol Scand 58:1127–1133.

Podobinska M, Szablowska-Gadomska I, Augustyniak J, Sandvig I, Sandvig A, Buzanska L (2017) Epigenetic modulation of stem cells in neurodevelopment: the role of methylation and acetylation. Front Cell Neurosci 11:1–16.

Popova S, Lange S, Burd L, Rehm J (2012) Health care burden and cost associated with fetal alcohol syndrome: based on official Canadian data. PLoS One 7:e43024.

Popova S, Lange S, Probst C, Parunashvili N, Rehm J (2017) Prevalence of alcohol consumption during pregnancy and Fetal Alcohol Spectrum Disorders among the general and Aboriginal populations in Canada and the United States. Eur J Med Genet 60:32–48.

Portales-Casamar E, Lussier AA, Jones MJ, MacIsaac JL, Edgar RD, Mah SM, Barhdadi A, Provost S, Lemieux-Perreault L-P, Cynader MS, Chudley AE, Dubé M-P, Reynolds JN, Pavlidis P, Kobor MS (2016) DNA methylation signature of human fetal alcohol spectrum disorder. Epigenetics Chromatin 9:25.

Resendiz M, Mason S, Lo CL, Zhou FC (2014) Epigenetic regulation of the neural transcriptome and alcohol interference during development. Front Genet 5:1–15.

Reynolds JN, Weinberg J, Clarren S, Beaulieu C, Rasmussen C, Kobor M, Dube M-P, Goldowitz D (2011) Fetal alcohol spectrum disorders: gene-environment interactions, predictive biomarkers, and the relationship between structural alterations in the brain and functional outcomes. Semin Pediatr Neurol 18:49–55.

Rushing G, Ihrie RA (2016) Neural stem cell heterogeneity through time and space in the ventricular-subventricular zone. Front Biol (Beijing) 11:261–284.

Sheller B, Clarren SK, Astley SJ, Sampson PD (1988) Morphometric analysis of macaca nemestrina exposed to ethanol during gestation. Teratology 38:411–417.

Shen EY, Ahern TH, Cheung I, Straubhaar J, Dincer A, Houston I, de Vries GJ, Akbarian S, Forger NG (2015) Epigenetics and sex differences in the brain: a genome-wide comparison of histone-3 lysine-4 trimethylation (H3K4me3) in male and female mice. Exp Neurol 268:21–29.

Sival DA, Guerra M, den Dunnen WFA, Bátiz LF, Alvial G, Castañeyra-Perdomo A, Rodríguez EM (2011) Neuroependymal denudation is in progress in full-term human foetal spina bifida aperta. Brain Pathol 21:163–179.

Smith SM, Garic A, Flentke GR, Berres ME (2014) Neural crest development in fetal alcohol syndrome. Birth Defects Res C Embryo Today 102:210–220.

Subbanna S, Nagre NN, Shivakumar M, Umapathy NS, Psychoyos D, Basavarajappa BS (2014) Ethanol induced acetylation of histone at G9a exon1 and G9a-mediated histone H3 dimethylation leads to neurodegeneration in neonatal mice. Neuroscience 258:422–432.

Subbanna S, Shivakumar M, Umapathy NS, Saito M, Mohan PS, Kumar A, Nixon RA, Verin AD, Psychoyos D, Basavarajappa BS (2013) G9a-mediated histone methylation regulates ethanol-induced neurodegeneration in the neonatal mouse brain. Neurobiol Dis 54:475–485.

Sulik KK (2005) Genesis of alcohol-induced craniofacial dysmorphism. Exp Biol Med 230:366–375.

Wilhelm CJ, Guizzetti M (2016) Fetal alcohol spectrum disorders: an overview from the glia perspective. Front Integr Neurosci 9:1–16.

Zarrei M, Hicks GG, Reynolds JN, Thiruvahindrapuram B, Engchuan W, Pind M, Lamoureux S, Wei J, Wang Z, Marshall CR, Wintle RF, Chudley AE, Scherer SW (2018) Copy number variation in fetal alcohol spectrum disorder. Biochem Cell Biol 96:161–166.

Zhang J, Parvin J, Huang K (2012) Redistribution of H3K4me2 on neural tissue specific genes during mouse brain development. BMC Genom 13: S5.

Zhou FC (2012) DNA methylation program during development. Front Biol (Beijing) 7:485–494.

Zhu Y, Sousa AMM, Gao T, Skarica M, Li M, Santpere G, Esteller-Cucala P, Juan D, Ferrández-Peral L, Gulden FO, Yang M, Miller DJ, Marques-Bonet T, Imamura Kawasawa Y, Zhao H, Sestan N (2018) Spatiotemporal transcriptomic divergence across human and macaque brain development. Science 362:1–15.

## SUPPORTING INFORMATION

Additional supporting information may be found online in the Supporting Information section at the end of the article.

**Appendix S1.** Published epigenetic studies of brain tissue following ethanol exposure.

**Table S1-1.** Changes in DNA cytosine modifications and related enzymes following experimental in utero (not postnatal) alcohol exposure in the brain specifically.

**Table S1-2.** Histone post-translational modifications (PTMs) and enzymes associated with experimental in utero (not postnatal) alcoholexposure in the brain specifically.

**Appendix S2.** Experimental details of macaque PNAE model.

**Table S2-1.** Alcohol-exposed and control macaque details [1–3].

**Appendix S3.** Rationale for the selection of epigenetic marks (DNA cytosine modifications, histone acetylation and histone methylation) being investigated in PNAE human and macaque monkey brain samples.

**Appendix S4.** Procedural details of immunohistochemical labeling.

**Appendix S5.** Immunohistochemical stains showing total histone H3 and H4 epigenetic modifications.

**Figure S5-1.** Representative immunohistochemical detection of epigenetic marks in human control temporal neocortex showing discrepancies between selective and total histone antibodies.

**Figure S5-2.** Representative immunohistochemical detection of epigenetic mark H3K36me3 in human control ventricular (VZ) and subventricular zones (SVZ).

**Figure S5-3.** Representative immunohistochemical detection of epigenetic marks in human control vascular endothelial cells, arterial smooth muscle cells lining blood vessels, and epithelial cells of the choroid plexus.

**Appendix S6.** Proportion rank values representing specific brain cell types among the temporal ependyma, dentate

gyrus, temporal cortex and white matter in human control fetal and infant cases for each of the epigenetic marks studied.

**Appendix S7.** Representative photomicrographs showing immunohistochemical detection of 5fC and H3K27me3 epigenetic marks in control and PNAE macaque temporal horn ependyma.

**Appendix S8.** Lack of immunohistochemical evidence for oxidative damage in human and monkey brains with prenatal alcohol exposure.